The effects of μ-opioid receptor agonists and antagonist in the pontine parabrachial nucleus on breathing patterns of decerebrate canines

Prkić, Ivana

UNIVERSITY OF SPLIT
SCHOOL OF MEDICINE

Ivana Prkić, M.D.

THE EFFECTS OF μ-OPIOID RECEPTOR AGONISTS AND ANTAGONIST IN THE PONTINE PARABRACHIAL NUCLEUS ON BREATHING PATTERNS OF DECEREBRATE CANINES

DOCTORAL THESIS

Mentor: Edward J. Zuperku, Ph.D.

May, 2015

ABBREVIATIONS

5-HT	serotonin
aCSF	artificial cerebrospinal fluid
BC	Bötzinger complex
BPM	breaths per minute
cAMP	cyclic adenosine monophosphate
CNS	central nervous system
cVRG	caudal part of the ventral respiratory column
DAMGO	[D-Ala2, N-Me-Phe4, gly-ol5]-enkephalin
DOR	δ-opioid receptors
DRG	dorsal respiratory group
E	expiratory
E-Aug	expiratory augmenting
E-Con	expiratory constant
E-Dec	expiratory decrementing
f_B	breathing frequency
GPCR	G protein coupled receptors
I	inspiratory
I-Aug	inspiratory augmenting
IC	inferior colliculi
I_{CAN}	calcium-activated non-selective cationic current
I-Con	inspiratory constant
I-Dec	inspiratory decrementing
I_{NaP}	persistent Na^+ current

KF	Kölliker Fuse nucleus
KOR	κ-opioid receptors
kPa	kilo Pascal
MOR	μ-opioid receptors
MOR-ir	μ-opioid receptor immunoreactivity
NAL	naloxone
NK1	neurokinin-1
NK1R	neurokinin-1 receptor
NORt	nociception orphanin FQ peptide receptor
NRM	non-respiratory modulated
NTS	nucleus of the solitary tract
PB-KF	parabrachial/Kölliker-Fuse
PBN	parabrachial nuclei
PBS	phosphate-buffered saline
pFRG	parafacial respiratory group
PKA	protein kinase A
PNG	phrenic neurogram
PPA	peak phrenic activity
preBC	preBötzinger complex
PRG	pontine respiratory group
remi	remifentanil
RTN	retrotrapezoid nucleus
RTN/pFRG	retrotrapezoid nucleus/parafacial respiratory group
rVRG	rostral ventral respiratory group
SP	supstance P

T_E	expiratory time
T_I	inspiratory time
TRH	thyrotropin releasing hormone
VRC	ventral respiratory column
VRG	ventral respiratory group
V_t	tidal volume

Contents

1. INTRODUCTION

Morphine and synthetic μ-opioid receptor (MOR) analogs are highly effective analgesics in humans and mammals. They can be used to treat both acute severe perioperative pain (e.g., fentanyl, sufentanil, remifentanil) as well as severe chronic pain states (e.g., morphine and fentanyl). The most serious, potentially life-threatening side effect of opioids is the depression of breathing, which can occur at clinically relevant analgesic plasma concentrations. This is particularly common during recovery from surgical anesthesia when supplemental doses of μ-opioid agonists are required for pain control and the patients' level of consciousness can frequently and rapidly alternate between consciousness and sleep/deep sedation.

Profound respiratory depression is clinically manifested by marked slowing of the respiratory rate leading to bradypnea or even apnea often accompanied by upper airway obstruction. These respiratory depressant effects are thought to originate within the pontomedullary respiratory rhythm and pattern-generating region, where opioid receptors have been identified on neurons throughout these nuclei, including those in the preBötzinger Complex (preBC), the putative locus for rhythm generation (1).

Based on *in vitro* studies in reduced brainstem preparations and immunohistochemical analysis, which suggest a direct opioid effect on structures within the preBC, it is generally accepted that systemically administered opioids act within the preBC to cause respiratory depression. However, a recent study showed that extensive bilateral microinjections of the opioid antagonist naloxone (NAL) into the preBC region did not reverse the bradypnea induced by intravenous infusions of remifentanil (remi) at clinically relevant concentrations in decerebrate dogs (2). Moreover, direct microinjections of the MOR agonist into the preBC region in decerebrate dogs resulted in tachypnea rather than bradypnea (2). Evidence from these *in vivo* studies suggested that the clinically observed, μ-opioid-induced bradypnea occurs at sites outside of the preBC (3-7).

Other regions of the respiratory control system also exhibit high densities of MORs and may be more sensitive to systemic opioids than the preBC. One such region is the parabrachial complex in the dorsal lateral pons, where earlier studies showed a depressive effect by opioids in or near this region (8). The purpose of the present studies was to more precisely define the pontine region in which MOR agonists produce bradypnea and to determine whether antagonism of MORs in that region reverses the bradypnea produced by systemic administration of clinically relevant concentrations of the MOR agonist remi.

1.1. Central Mechanisms in the Control of Breathing

Breathing is physiological process generated and controlled by the central nervous system (CNS). It is required to sustain life through the maintaining blood and tissues concentrations of oxygen and carbon dioxide. Breathing is the only mammalian behavior that requires continuous movement of skeletal muscles and it consumes ~7% of metabolic output at rest (9). Respiratory neurons that are involved in breathing are arranged as a bilateral column in the brainstem from the rostral pons to the caudal medulla. Respiratory rhythm is established via synaptic interactions between these neurons and their connections with cranial and spinal motoneurons and interneurons (10). The role of the brain in breathing is preeminent, as it generates the motor outflow driving the contraction and relaxation of skeletal muscles that pump the lung and modulate the tone of skeletal and smooth muscles in the upper airway and bronchi to control resistance to air flow (11). Our breathing follows a rhythm that can have up to three phases. The first phase called "inspiration" begins when we breathe in. During the second phase, which is called "post-inspiration", air is slowly leaving the lungs. Post-inspiration is particularly important for generating speech. During the third phase, that is called "active expiration", other muscles contract to actively push air out of the lungs. Active expiration is important during exercise, but it is not necessary under resting conditions (12).

Breathing is also an essential component of many vocal and emotive behaviors including, e.g., crying, sniffing, laughing and singing, and must be coordinated with such vital behaviors (9) to meet our metabolic and environmental needs.

1.2. Respiratory neurons

Respiratory neurons are concentrated within three brainstem regions: the dorsal respiratory group (DRG) within the nucleus of the solitary tract, the ventral respiratory column (VRC) and pontine respiratory group (PRG) (Fig. 1).

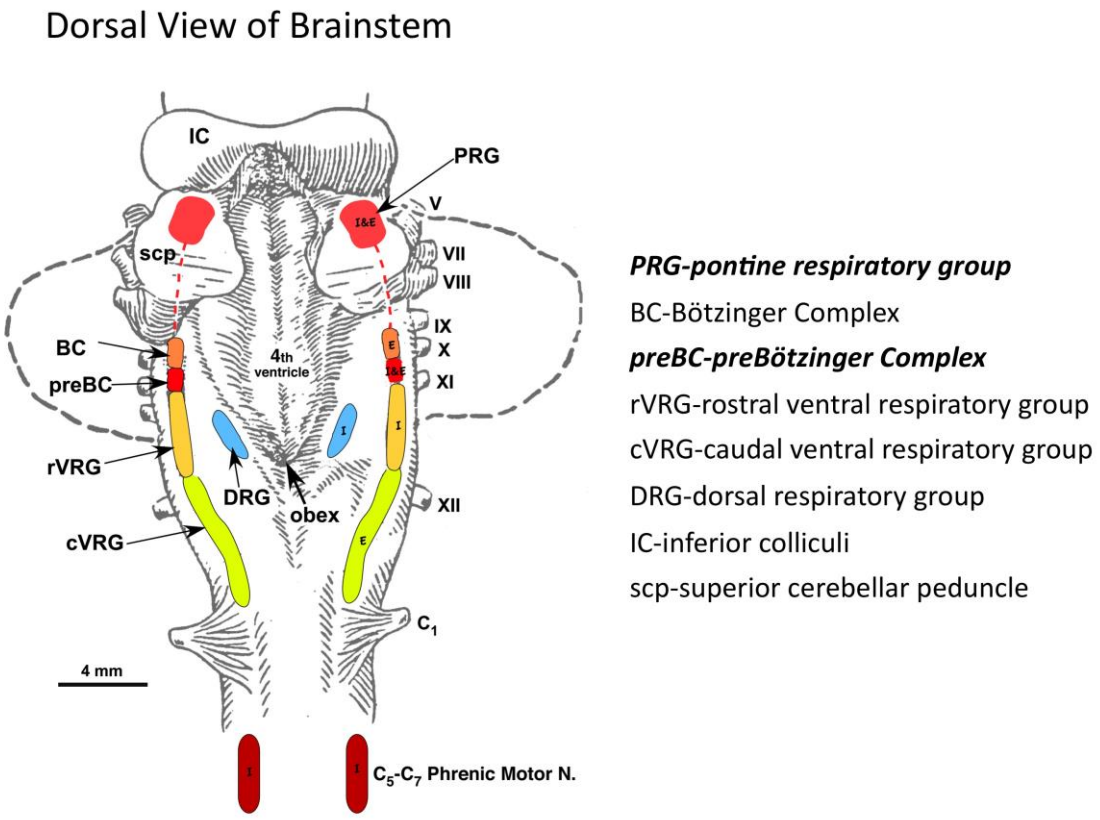

Figure 1. Dorsal view of the brainstem with groups of respiratory neurons.

These respiratory clusters together with respiratory-related sensory afferents are responsible for the automatic control of breathing and adaptive changes in breathing to homeostatic and environmental challenges (13). Breathing is maintained and adjusted to our metabolic, behavioral and environmental needs. Despite its complexity, breathing is controlled by a very small network of neurons within the brainstem (14).

Pontomedullary respiratory neurons receive modulatory synaptic input from non-respiratory regions that include the motor cortex, hypothalamus, reticular formation, cerebellum, limbic and cardiovascular regions of the brainstem and extrapyramidal motor areas. These non-respiratory modulatory inputs adapt breathing rhythm and pattern for effective cardio-respiratory interactions and activities such as phonation, swallowing, coughing, physical exertion, defecation and postural change (10).

The nomenclature of respiratory neurons follows from the phase in which their bursting activity occurs. Thus, neurons are designated as inspiratory (I), expiratory (E) and phase-

spanning. There are usually categorized by their characteristic augmenting (I-Aug, E-Aug), decrementing (E-Dec, I-Dec) or relatively constant (E-Con, I-Con) firing patterns, and by firing patterns that either span the boundaries between inspiratory and expiratory phases (E-I, I-E) or which fire only during subportions of the respiratory phases.

Neuromodulators affect discharge pattern of all respiratory neurons. Modulators that alter respiratory rhythm and pattern include: catecholamines, serotonin, acetylcholine, adenosine and peptides including substance P (SP), neuropeptide Y, cholecystokinin, met-enkephalin, galanin and thyrotropin-relasing hormone (TRH).

1.2.1. The dorsal respiratory group

The dorsal respiratory group (DRG, Fig. 1, blue) is located in the dorsomedial medulla caudal to mid-rostral portions of the nucleus of the solitary tract (NTS). The dorsal respiratory group includes mainly inspiratory (I) bulbospinal neurons (neurons that project to spinal motoneurons, which in turn innervate the respective respiratory pump and abdominal muscles of breathing) but also propriobulbar neurons (neurons that project to other medullary respiratory neurons and influence their activity but themselves do not project to motoneurons *per se*), P cells (neurons which fire in phase with lung inflation) and few expiratory (E) propriobulbar neurons (15). It is a source of input of respiratory motoneurons in some species, but less in others.

The NTS provides the first step in the brain's processing of critical information about the status of lungs and airways (16), as well as sensory input from peripheral chemoreceptors detecting arterial O_2 and CO_2 (13). Some inspiratory premotoneurons and propriobulbar neurons of the DRG might be involved in nonrespiratory motor activities like swallowing and coughing (17).

1.2.2. The ventral respiratory column

The ventral respiratory column (VRC) forms a continuous field in the ventrolateral medulla extending from the spinomedullary junction to the facial nucleus. It contains bulbospinal respiratory premotoneurons that receive converging inputs from VRC rhythm generating neurons outside the VRC, sculpting the activity pattern distributed to various pools of respiratory neurons.

It is divided into six distinct sub-regions from caudal to rostral: the caudal ventral respiratory group (cVRG, Fig. 1, green), the rostral ventral respiratory group (rVRG, Fig. 1, orange), the preBC (Fig. 1, red), the Bötzinger complex (BC, Fig. 1, dark orange), the parafacial respiratory group (pFRG) and the retrotrapezoid nucleus (RTN) (18). These sub-regions are clusters of similar types of respiratory neurons each active during a particular phase of the respiratory cycle (e.g. inspiratory, expiratory or mixture of both (13)).

Respiratory rhythm generation occurs mainly in the rostral half of the VRC (19, 20) and bulbospinal neurons in the caudal half of the VRC modulate the amplitude of respiratory motor output on spinal respiratory nerves (13).

1.2.2.1. Caudal ventral respiratory group

The cVRG extends from the obex just to the nucleus ambiguous to the spinal medullary border. It contains bulbospinal respiratory premotoneurons with a firing pattern that increases during expiration. They are mainly excitatory and project to motoneurons and interneurons innervating thoracic and upper motoneurons that drive expiratory pump muscle (internal intercostal and abdominal muscles) (18). Inhibitory expiratory neurons in the cVRG and in the vicinity of the BC inhibit spinal inspiratory motor pools (11).

1.2.2.2. Rostral ventral respiratory group

The rVRG contains the excitatory bulbospinal inspiratory neurons (I-Aug). Glutamate and enkephalin are likely co-transmitters for bulbospinal I-Aug neurons (21). Inspiratory bulbospinal neurons project monosynaptically to inspiratory motoneurons in the phrenic nucleus in the cervical spinal cord and to external intercostal motoneurons in the thoracic spinal cord (22, 23).

The rVRG includes substantial population of respiratory neurons that project locally within the brainstem and particularly within the medulla (13). Neurons related to respiratory rhythm formation are located in several adjacent compartments, including the most anterior portions of the rVRG, the preBC, and possibly elements of the RTN.

The anterior portion of the rVRG contains a distinctive population of I-Aug bulbospinal neurons that have neurokinin-1 (NK1) receptors and modest differences in their firing pattern (23). These neurons distinguish from nearby NK1 receptor (NK1R) positive propriobulbar

neurons in the preBC by their spinal projections and size (23), as well as by their I-Aug firing pattern as compared to the E-I pattern common in preBC neurons.

1.2.2.3. The preBötzinger complex

The preBC is located at the rostral end of this VRC, between the BC and rVRG. This region was identified *in vitro* and *in vivo* as a medullary region essential for respiratory rhythm generation (24-26). The preBC consists of neurons whose *in vivo* firing patterns spans the temporal boundaries between the expiratory and inspiratory phases of the respiratory cycle (27). The preBC isolated in medullary slices, continues to generate three distinct types of activity patterns that appear to provide the basic rhythmic drive for the generation of three forms of respiratory activity patterns: normal respiratory activity, sighs and gasps (28).

Bursting preBC neurons have two underlying ionic mechanisms. The first is voltage-sensitive and depends on subthreshold activation of persistent Na^+ current (I_{NaP}) in neurons with sufficiently low leakage-like K^+ current (29-32) that are present in a subset of preBC neurons as well as within the medulla and it is not a specialized property of preBC neurons (31-33). The second mechanism depends on a Ca^{2+}-activated nonspecific cationic current (I_{CAN}) (34) whose activation mechanism in the absence of synaptic input depends on voltage-gated Ca^{2+} channels. Bursting of this type is less voltage-sensitive (35, 36). Pacemaker bursting in one population of inspiratory neurons seems to depend on the I_{CAN}. These neurons are referred to as "cadmium-sensitive" pacemaker neurons, because bursting in these neurons is abolished following blockade of calcium influx with extracellularly applied cadmium. Pacemaker bursting in the other population of inspiratory neurons seems to depend on the persistent sodium current. These neurons are referred to as "cadmium-insensitive" pacemaker neurons, because bursting in these neurons continues even following blockade of calcium currents with extracellularly applied cadmium. Neuromodulators that cause a frequency and regularity increase in respiratory network activity evoke a frequency increase specifically in the endogenous bursting of isolated cadmium-insensitive pacemakers. Under normal conditions the two types of pacemaker neurons are active and both excitatory and inhibitory synaptic mechanisms are critical for rhythm generation (36).

The preBC circuit has two basic functions: a) generation of rhythmic excitatory inspiratory drive, including the pre-I component of this drive that is important for initiation of the inspiratory phase; and b) coordination of inspiratory-expiratory pattern formation via

inspiratory inhibition provided by the preBC inhibitory neurons (37). The core mechanism for rhythm generation is an "inhibitory ring" of three distinct neuronal populations of preBC and BC neurons that sequentially inhibit each other and transform a presumptive tonically active subpopulation of excitatory preBC neurons into an inspiratory-modulated one (38-40). The primary role of inhibition appears to be in shaping the pattern of respiratory motor output and assuring its stability, but not in the generation of rhythm *per se* (9).

A subset of neurons within the preBC expresses the NK1R for which SP is ligand and they are assumed to be rhythm-generating neurons. The presence of these neurons was proposed to identify the preBC (1). Within the preBC, SP is primarily co-localized with glutamate, but to lesser degree also with GABA (41).

Under most experimental conditions in slices from neonatal rodents, ~5–25% of all preBC inspiratory neurons exhibit bursting pacemaker properties, regardless of transmitter phenotype being glutamatergic or glycinergic (31, 35, 42-44). NK1R are prominent in the preBC but also in numerous other structures as ventrolateral medulla including BC and RTN. Newer data demonstrate that pacemakers and their underlying intrinsic conductance can contribute to rhythmogenesis but they are not essential (31, 40, 45).

GABA-B and μ-opioid receptors (MORs) are co-localized on preBC neurons that express the NK1Rs (1). When activated, MORs reduce excitability of NK1 preBC neurons (1). A functional antagonist of the MOR-signaling pathway in preBC neurons is the 5HT4 receptor, which does not appear to be present in pain pathways (46). A subpopulation of preBC neurons also expresses somatostatin, a neuropeptide that has a modulatory action on breathing (47).

The preBC receives multiple modulatory inputs from many areas outside and within the vicinity of the preBC. The connectivity amongst preBC neurons must play an essential role in the stability and lability of the rhythm, and probably in rhythmogenesis too. Regions that are well known for their important modulatory roles are raphe magnus and obscures. These regions contain a variety of neurotransmitters and neuromodulators including GABA, serotonin (5-HT), SP and TRH (36). All these areas either receive input from or project to the preBC (48). There are also important connections between preBC and retrotrapezoid nucleus/parafacial respiratory group (RTN/ pFRG), ventral respiratory column caudal to preBC, parahypoglossal nucleus, nucleus of the solitary tract, PRG and periaqueductal gray (49).

1.2.2.4. The Bötzinger complex (BC)

The BC is located between preBC and facial nucleus. It contains mainly inhibitory glycinergic expiratory neurons (50). GABAergic inputs are more dominant than glycinergic inputs to inspiratory bulbospinal neurons during the expiratory phase of breathing in dogs (51). It seems that the BC is one of the most likely sources of expiratory inhibitory afferents (13) and it has been shown to provide widespread inhibitory projections within the VRC with E-Aug neurons targeting inspiratory and expiratory bulbospinal neurons, as well as substantial number of respiratory-related cranial motoneurons (13). A subset of BC neurons sends axons rostrally, targeting the facial nucleus RTN, respiratory-related areas of the pons, and dorsally to the NTS and to spinal inspiratory motor pools. The BC neurons are critically involved in the control of the transition between inspiratory and expiratory activities in the network, which is fundamental for the rhythmic inspiratory-expiratory alternation essential for normal breathing (37).

1.2.2.5. The retrotrapezoid nucleus/the parafacial respiratory group

The retrotrapezoid nucleus (RTN) is located at the rostral end of the VRC, ventral to the BC and continues rostrally beneath the facial nucleus near the surface of the brain to just caudal to the trapezoid body.

The RTN has been shown to be an important area of central chemoreception (52-54). The discharge frequency of RTN neurons greatly depends on the pH of the surrounding tissue and $PaCO_2$. RTN function appears to be inhibited by GABA-A agonists (55). The RTN is a region containing potential central chemosensory cells, an important source of respiratory drive and chemoreflexes. RTN neurons project to the pons and caudal VRC and their neuronal activity increases with extracellular acidity.

The preBC and RTN/pFRG have been identified in reduced neonatal rodent preparations as potentially coupled inspiratory and expiratory rhythm generating centers with pacemaker neurons (20, 56).

The parafacial respiratory group (pFRG) is ventral to the facial nucleus. The RTN/pFRG contains neurons that are sensitive to the brain carbon dioxide level and receives input from peripheral chemoreceptors. The RTN provides chemosensitive excitatory drives to most of the respiratory network and adapts the activity to the metabolic state of system (37). This area may play an important role in rhythm generation.

1.2.3. Pontine respiratory group

The pontine respiratory group (PRG, Fig. 1, red) is positioned in the rostral dorsolateral pons and includes portions of the parabrachial nucleus (PBN) and the ventrally adjacent Kölliker-Fuse (KF) nucleus.

A variety of respiratory neuronal types have been found in this region, including inspiratory (I), expiratory (E) and phase-spanning patterns (57-59). In this region are also found non-respiratory related neurons, which show tonic activity patterns (57). Zuperku et al classified PRG neurons of adult dog into seven distinct subgroups based on their discharge patterns (60).

It appears that KF neurons are under a potent GABAergic inhibitory control. NMDA receptors have been localized in the dorsolateral pons (61). Glutamatergic receptors are also found on pontine respiratory neurons and may be potential targets for anesthetic depression of respiratory function. Also, KF area represents a mandatory relay for the nasotrigeminally induced apnea and bradycardia that are mediated by NMDA receptors in the KF (62).

The KF is the source of the most massive projections to the VRC and projections to the respiratory-related areas of the NTS, as well as to the hypoglossal and facial nuclei (59). The major respiratory-related projections to this area are from NTS and from the VRC (63).

Pontine connections to the caudal medullary circuits seem to be important for coordinating the activity of expiratory muscles and upper airway musculature during expiration and for expression and regulation of post-inspiratory activity. Respiratory-related neurons in the pons play an important role in shaping the activity of medullary respiratory neurons during the breathing cycle (40, 64) and the activity patterns of pontine respiratory neurons are altered by sleep–awake states (65).

1.3. The opioids

Opioids are chemicals that resemble morphine or other opiates in its pharmacological effects. They have been used for pain relief over thousands of years and are still the most effective analgesics used for the control of acute and chronic pain. The term opiate is limited to the natural alkaloids found in the resin of the plant *Papaver somniferum* (opium poppy), while opioid refers to both opiates and synthetic substances and opioid peptides. Opioids act by attaching to specific receptors, which are located in the central and peripheral nervous system

and the gastrointestinal tract. The receptors in these organ systems mediate the beneficial effects as well as the side effects of opioids. When opioids attach to their receptors, they inhibit the presynaptic release and postsynaptic response to excitatory neurotransmitters from nociceptive neurons. The effect of specific opioid depends on which receptor is bound and the binding affinity of the drug (66).

Opioids have many side effects that include sedation, constipation, drowsiness, nausea, vomiting, itch, tolerance, addictive behaviors and strong sense of euphoria (67). The most serious, potentially fatal acute side-effect of opioid analgesics is respiratory depression, which can occur at clinically relevant analgesic plasma concentrations. Profound respiratory depression limits the use of opioid analgesia and it is clinically manifested by slowing of the respiratory rate leading to bradypnea or even apnea often accompanied by upper airway obstruction. The incidence of postoperative opioid-induced respiratory depression in the UK has been estimated to be approximately 1% (68). It is, however, unclear which sites in the brain are responsible for opioid-induced respiratory depression (69).

1.4. The opioid receptors

There are four classes of opioid receptors: the μ (MOR), κ (KOR), δ (DOR), and the nociceptin/orphanin FQ peptide receptor (NOR) (70, 71). The ligands for these receptors are endogenous peptides and alkaloids that include opioid agonists and antagonists.

Endogenous peptides are: the endorphins (attach to the MOR), enkephalins (attach to the DOR and MOR), the dynorphins (attach to the KOR), and nociceptin/orphanin FQ (attach to the NOR) (69). Endogenous opioid peptides are small molecules that are naturally produced in the central nervous system and in various glands throughout the body in states of stress or exercise. These peptides function both as hormones and neuromodulators that can block the transmission of pain signals (66). The endogenous opioid system mediates many physiological effects, including pain, respiratory control, stress responses, appetite, and thermoregulation.

Opioid receptors are most abundant in the CNS primarily in the cortex, limbic system and brainstem but have also been localized in many peripheral tissues of the mammalian organism (72) including carotid bodies and mechanosensory receptors in the lungs (69). Immunoreactivity for MOR, KOR and DOR was found in respiratory-related regions of the brain stem and spinal cord (10).

Binding sites for the three opioid receptors overlap in most structures, but some structures exhibit higher expression of one receptor over the others (67).

Pain relief effects are mediated by three receptor types (MOR, KOR, DOR), but in different degree. MOR mediates the most potent antinociceptive effects, accompanied by the development of dependence. MORs are located throughout the central nervous system in areas like neocortex, caudate putamen, nucleus accumbens, thalamus, hippocampus, amygdala, nucleus of the solitary tract, dorsal horn of the spinal cord and periaqueductal grey. DOR has a lower efficacy in mediating pain relief but also a reduced addictive potential. KORs mediate analgesic effects in peripheral tissues and are also involved in feeding and neuroendocrine function (5).

1.4.1. G protein coupled opioid receptors

Opioid receptors belong to the big family of G-protein coupled receptors that share the similar seven-transmembrane topology. G-protein coupled receptors have no direct link with effector proteins; instead the message is relayed via a G-protein that consists of three subunits: α, β and γ. When a G protein coupled receptor (GPCR) agonist binds to the extracellular domain, it induces a change in conformation of the receptor. This leads to coupling and activation of one or more G proteins inside the cell (73).

Activation of opioid receptors by agonists leads to intracellular signaling cascade that mediates the actions of many hormones and neurotransmitters (69). This cascade includes: (a) closing of voltage sensitive calcium channels; (b) stimulation of potassium efflux leading to hyperpolarization; and (c) reduced cyclic adenosine monophosphate (cAMP) production via inhibition of adenylyl cyclase. Overall, this results in reduced neuronal cell excitability leading to a reduction in transmission of nerve impulses along with inhibition of neurotransmitter release (74).

1.5. Possible sites for opioid-induced respiratory depression

Opioid analogs are highly effective analgesics in humans and mammals. The most serious side effect of opioids is potentially life-threatening depression of breathing, which can occur at clinically relevant analgesic plasma concentrations. This is particularly common during recovery from surgical anesthesia, when supplemental doses of MOR agonists are required for pain control and the patients' level of consciousness can frequently and rapidly alternate

between consciousness and sleep/deep sedation. Profound respiratory depression is clinically manifested by marked slowing of the respiratory rate leading to bradypnea or even apnea often accompanied by upper airway obstruction. A decrease in respiratory rate and tidal volume (V_t) can be observed during experimentally controlled isocapnic conditions. These respiratory depressant effects are thought to originate within the pontomedullary respiratory rhythm and pattern-generating region and possibly in other brain stem regions including NTS, VRC and the lateral pons (3-7). Opioid receptors have been identified on neurons throughout these nuclei, including those in the preBC, the putative locus for rhythm generation. With localized application of MOR agonists, the discharge activity of many brain stem respiratory neurons can be reduced or entirely abolished (3, 10, 48, 75). Since several studies have used local microinjections of MOR agonists at concentrations much greater than those obtained via systemic administration in a clinical dose range, it is possible to incorrectly assign the role of MORs in a specific location to producing an observed clinical effect. A more reliable method to evaluate the role of MORs at a specific location within the control network would be to test the ability of a locally applied antagonist to reverse the effect of the systemically applied agonist. In vitro studies using bath application of opioids in reduced brain stem preparations (1) and studies using immunohistochemical techniques (46, 76) provide strong evidence for a direct opioid effect on structures within the preBC. This has led investigators to suggest that MORs in the preBC may be major contributors to the bradypnea produced by systemically administered opioids (10, 46, 77, 78). In addition, other sites within the pontomedullary respiratory system including the rostral pons have been suggested as potential targets by some of these investigators. However, a recent study showed that extensive bilateral microinjections of the opioid antagonist naloxone (NAL) into the preBC region did not reverse the bradypnea induced by intravenous infusions of remifentanil (remi) at clinically relevant concentrations in decerebrate dogs (2). Moreover, direct microinjections of the MOR agonist [D-Ala2,N-Me-Phe4,Gly5-ol] enkephalin acetate (DAMGO) into the preBC region in decerebrate dogs resulted in tachypnea rather than bradypnea (2). Microinjections of the selective MOR agonist endomorphin-1 into the preBC region of anesthetized rats also produced a tachypneic response (76). Evidence from these *in vivo* studies suggests that the clinically observed μ-opioid-induced bradypnea occurs at sites outside of the preBC. There are other regions of the respiratory control system besides the preBC that exhibit high densities of MORs, and these may be more sensitive to systemic opioids than the preBC (6, 79). High densities of MOR immunoreactivity (MOR-ir) have been found in the parabrachial/Kölliker-Fuse (PB-KF)

region of rats (80, 81) and cats (7). In fact, Hurle et al. (1985) found that μ- and δ-opioids applied to the dorsal surface of the pons near the PB region of cats produced a profound decrease in breathing rate with no change in tidal volume. In contrast, bilateral localized application to the ventral surface of the medulla resulted in a reduction in tidal volume and response to CO_2 and an increase in breathing rate (8). In addition, Eguchi et al. (1987) found that microinjections of morphine into the PBN of anesthetized, vagotomized, paralyzed, and artificially ventilated cats produced a marked decrease in phrenic neurogram (PNG) burst rate (82). This evidence led us to perform exploratory experiments in decerebrate dogs as described below, which showed that pledgets saturated with DAMGO and applied to the dorsal surface of the pons between the inferior colliculi (IC) and superior cerebellar peduncles caused a profound bradypnea without any change in peak phrenic nerve activity (PPA). Consistent with those findings, immunohistochemical mapping of MORs in one dog showed high levels of MOR-ir in the region of the lateral PBN. Lalley's studies suggest that slowing occurs either in the preBC or the pons while Mustapic et al. results suggest that the preBC is not involved, which leaves the pons as the major target of opioid-induced slowing as observed with supraclinical opioid agonist concentrations in a feline model by Hurle at al 1985 (8, 10).

Thus, hypothesis of this study is that clinically relevant concentrations of MOR agonists cause reduction in respiratory rate (bradypnea) via activation of pontine MORs. The purpose of the present study was to more precisely define the pontine region in which MOR agonists produce bradypnea and to determine whether antagonism of MORs in that region reverses the bradypnea produced by systemic administration of clinically relevant concentrations of the MOR agonist remi.

2. RATIONALE, OBJECTIVES AND HYPOTHESIS

The rationale of the study is:

A first step in understanding how systemic opioids induce depression of breathing is to determine the location(s) within the respiratory network where this effect takes place.

The objectives of this study are:

a) to define the pontine region in which MOR agonists produce bradypnea, and
b) to determine whether antagonism of MORs in this region reverses the bradypnea produced by systemic administration of clinically relevant concentrations of the MOR agonist remi.

The hypothesis is:

Clinically relevant concentrations of MOR agonists cause reduction in respiratory rate (bradypnea) via activation of pontine MORs.

3. METHODS

This study was approved by the subcommittee on animal studies of the Zablocki Veterans Affairs (VA) Medical Center, Milwaukee, WI, USA, in accordance with provisions of the Animal Welfare Act, the *Guide for the Care and Use of Laboratory Animals*, and the institutional policy. Experiments were performed on 35 beagle dogs of either sex, weighing from 9 to 12 kg. Inhalational anesthesia was induced by mask and maintained with isoflurane (*Abbott, Chicago, IL, USA)* at 1.5-2.5% end-tidal concentration. The animals were monitored for signs of inadequate anesthesia such as salivation, lacrimation, and increase in blood pressures and heart rate. If required, anesthetic depth was increased immediately.

3.1. Surgical procedures

Anesthesia was induced by mask with isoflurane and the dogs were intubated with a cuffed endotracheal tube and their lungs were mechanically ventilated with an air-O_2-isoflurane mixture. End-tidal CO_2 concentration was continuously recorded with an infrared analyzer (*POET II, Criticare Systems Waukesha, WI, USA*). The femoral artery was cannulated for blood pressure recording and blood gas sampling (*Gould-Statham P23 ID transducer, Oxnard, CA, USA*) and the femoral vein for continuous infusion of maintenance fluids (0.9% NaCl) and administration of drugs. If required, additional sodium bicarbonate was given to correct metabolic acidosis. The animals were positioned in a Kopf (*model 1530; David Kopf Instruments, Tujunga, CA, USA*) stereotaxic apparatus with the head ventrally flexed by 30º. The vertebral column was maintained straight through caudal tension applied via a hip-pin clamp. A bilateral pneumothorax was performed to minimize brain stem movement and phasic inputs from pulmonary stretch receptors. After a midline skin incision was made from the spinous process of the axis to the nasion, the muscles and underlying connective tissue were cut along the external sagittal and nuchal crests, dissected bilaterally, and reflected to expose the parietal bones from the midline to ~5 cm laterally and from the nuchal crests to ~5 cm rostrally. A high-speed drill with burr was used to drill the margins of exposed parietal bones to form 3.5-cm-long x 3.5-cm-wide bilateral craniotomy windows. Bone wax was applied to the cut bony edges to stop bleeding and to prevent potential air embolism. The dura was removed with scissors to expose the parietal and occipital lobes bilaterally. The animal was then decerebrated by midcollicular transection (83) and isoflurane was gradually discontinued. A bipolar coagulator (*model 0441010; Burton Division of Cavitron Corporation, Van Nuys, CA, USA*) with insulated bayonet forceps (*90-mm shaft, 2-mm tips;*

Edward Weck & Company, Research Triangle Park, NC, USA) was used to coagulate small volumes of brain tissue. With the sequential coagulation and suctioning of small amounts of the brain tissue, the caudal portions of the parietal and temporal lobes and the occipital lobe were removed bilaterally to expose the midbrain region. Cotton-tipped applicators were used for blunt dissection of midline brain structures under the falx and above the brain stem to expose the great cerebral vein and its main branches. The applicators were also used to identify the midcollicular line, which runs just in front of the vermis and the commissure of the inferior colliculi. The origins of the oculomotor nerves were identified bilaterally on the ventral surface of the rostral mesencephalon by using the applicator to gently elevate (2-3 mm) the brain stem. To facilitate brain stem transection in the desired plane, the edge of spatula was placed by the side of the brainstem, from just behind the origin of oculomotor nerve ventrally and tilted toward the midcollicular line dorsally, to serve as a guide for the scalpel. The last few millimeters of the ventral brain stem were cut gently to avoid damage to the cavernous sinuses. In case of bleeding, bleeding was stopped by gentle bipolar coagulation and with an absorbable hemostatic material, oxidized regenerated cellulose (*Surgicel, Johnson & Johnson Medical, New Brunswick, NJ, USA*). Complete access of the dorsal surface of the brain stem was obtained by an occipito-parietal craniotomy followed by cerebellectomy and external sagittal and nuchal bone crest removal. In a subset of dogs in protocol 2, studies were performed during isoflurane anesthesia without decerebration. The animals were ventilated with an air-O2 mixture and maintained in hyperoxic isocapnia (FIO_2 >0.6, end-tidal CO_2 range 40–50 mmHg). After bilateral neck dissections, phrenic nerve was placed on bipolar platinum electrodes in a mineral oil pool formed from a neck pouch and recorded from the desheathed right C5 rootlet. The PNG was obtained from the moving-time average (100 ms) of the amplified phrenic nerve activity and was used to produce timing pulses corresponding to the beginning and end of the inspiratory phase for the measurement of inspiratory duration (TI) and expiratory duration (TE). Peak phrenic activity (PPA) was also obtained from the PNG. The breath-by-breath fictive breathing rate [phrenic activity burst rate; f_B, breaths/min (BPM)] was calculated as 60/ (TI + TE). Continuous neuromuscular block was achieved with pancuronium bromide (*Hospira Inc., Lake Forest, IL, USA)* (0.1 $mg \cdot kg^{-1} \cdot h^{-1}$) to reduce motion artifacts during neuronal recordings. Bilateral vagotomy was performed to eliminate afferent vagal input from pulmonary stretch receptors to avoid interference of the mechanical ventilation with the underlying central respiratory rhythm and respiratory neuronal activity. Esophageal temperature was maintained at 38.5 ± 1°C with a servo-controlled heating pad.

Mean arterial pressure was maintained above 80 mmHg, if required, with adjustment of intravenous fluids and phenylephrine infusion (0.5–5 $\mu g \cdot kg^{-1} \cdot min^{-1}$).

3.2. Microinjection technique

A minimum of 1 h was allowed for preparation stabilization before data collection. A Hamilton microliter syringe (5 µl) with a calibrated scale (resolution: 50 nl) was used for microinjections of the MOR agonist DAMGO (100 µM) and the MOR antagonist NAL (100 µM) to locate MORs in the rostral pons that alter f_B. The relatively high concentrations of the MOR agonist [$_D$-Ala^2, N-Me-Phe^4, Gly-ol^5]-enkephalin (*DAMGO, 100 µM, Sigma Aldrich, St. Louis, MO, USA*), and the MOR antagonist naloxone (*NAL, 500 µM and 5 mM, Abbott, Chicago, IL, USA*), which were dissolved in artificial cerebrospinal fluid (aCSF), were used to saturate the MORs in a small region (~1-mm diameter) of the pons to map out the extent of the opioid-sensitive region. Remifentanil (remi) was not used for injection at high concentrations since the only available formulation contains glycine, which is in itself inhibitory to neurons and would have thus confounded the results.

3.3. Remifentanil infusion

Remi (*Abbott, Chicago, IL, USA*) is a pure µ-agonist analgesic drug. Remi effects are antagonized by NAL. The analgesic effect is mediated through coupling of a guanine nucleotide binding protein (G protein), which concomitantly results in a presynaptic inhibition of excitatory neurotransmitter release and in a postsynaptic inhibition of cyclic adenosine monophosphatase, suppression of voltage-sensitive calcium channels, and hyperpolarization of the postsynaptic membrane through increased potassium conductance.

Advantages of using remi are its rapid onset, short latency to peak effect and its rapid recovery, which is independent of dose rate and length of infusion (Fig. 2). These properties are due to remi's rapid metabolism by nonspecific esterases in the blood and tissues. Because it is short acting, remi must be continuously infused. The time to a 50% decrease of an effective site concentration after infusion is stopped, has been estimated to be ~4 min for remi and is independent of infusion duration (84). The range of clinically useful plasma concentrations in anesthesia is ~1-20 ng/ml (85). The short-acting MOR agonist remi was continuously infused intravenously at a rate of ~0.5 $\mu g \cdot kg^{-1} \cdot min^{-1}$, which is the analgesic dose that reduces the requirements of a volatile anesthetic to blunt surgical stimuli in humans and

dogs by 50% (86, 87). This infusion rate was adjusted to produce >60% reduction in f_B during hyperoxic isocapnia, which was maintained by mechanical ventilation.

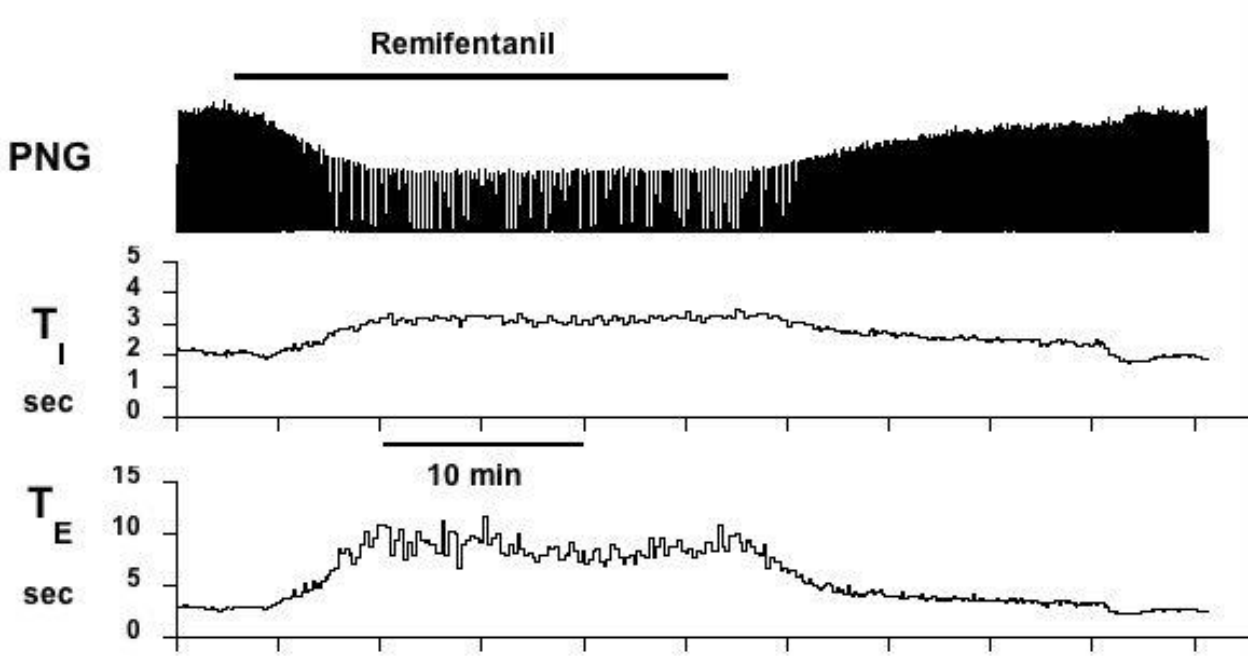

Figure 2. An example of remifentanil induced bradypnea. Remifentanil infusion (horizontal bar) produced an increase in inspiratory duration (T_I) and expiratory duration (T_E) and, in this case, a decrease in the peak phrenic neurogram (PNG). Note the rapid onset and recovery rates, which make it an ideal study drug for repeated trials in the same animal preparation.

3.4. Immunohistochemistry methods used for preliminary data

For immunohistochemical mapping of MOR, a carotid artery was cannulated rostrally in an anesthetized dog (n = 1) and perfused with phosphate-buffered saline (PBS) followed by 4% paraformaldehyde fixative with 0.2% picric acid in 0.1 M phosphate buffer. The brain was removed and postfixed in 4% paraformaldehyde fixative. Frozen transverse brain sections (25 μm) were cut from 10–17 mm rostral to the obex, and every fourth section was washed in PBS and incubated for 1 h in 5% normal goat serum in 0.3% Triton X-100 in PBS (PTX). Sections were then incubated in primary antibody, guinea pig anti- MOR-1 (1:3000 in 0.3% PTX; Millipore), for 24 h prior to Alexa Fluor 488-conjugated goat anti-guinea pig secondary (1:200; Invitrogen, Life Technologies, Grand Island, NY 14072 USA) for 1 h to yield a fluorescent signal for μOR. Sections were washed in PBS, floated onto slides, air-dried, dehydrated, and coverslipped. Control sections were processed simultaneously by incubation with serum instead of primary antibody and showed no staining for MOR. Sections were examined with a Nikon TE2000 microscope equipped for epifluorescence and photographed with an Optronics Quantifier 4 megapixel thermoelectrically cooled digital monochrome camera. Images were acquired at a resolution of 2,048 x 2,048 pixels with Optronics picture frame software and stored in TIFF format.

3.5. Preliminary study protocol: dorsolateral pons as a potential site of opioid-induced bradypnea

Studies in four dogs, with experimental procedures similar to those described above, were used to examine the possible involvement of the dorsolateral pons in opioid-induced bradypnea. Pledgets saturated with 100 μM DAMGO or 500 μM and 10 mM NAL were bilaterally placed on the dorsal surface of the pons between the IC and the superior cerebellar peduncle. The pledgets consisted of strands, three per side, of ~2-mm-diameter cotton string ~10 mm in length. They were submerged in a beaker containing either DAMGO or NAL so as to be completely saturated. During the protocol, they were exchanged about every 6 min during a ~30-min period to provide a continuous supply of the drug to the surface. After a maximum bradypneic response determined from the PNG, the dorsal pontine surface was rinsed with saline and NAL pledgets were then applied and exchanged as above to reverse the DAMGO-induced effect.

3.6. Injection protocols

Protocol 1: Respiratory effects of direct pontine μOR activation via pontine microinjection of DAMGO.

In a first series of animals (n = 10), pontine microinjections of DAMGO were used to define the regions that mediate opioid-induced bradypnea. A 5-μl Hamilton syringe was stereotaxically positioned over the dorsal surface of the pons, between the IC and superior cerebellar peduncles. A series of injections of DAMGO (100 μM, 300–500 nl each), ~10 min apart, were given covering 1 mm x 1 mm grids over a region from 4 to 8 mm lateral of midline and extending from 1 mm rostral to the caudal pole of the IC to 3 mm caudal to that pole at a depth of 3–4 mm from the dorsal surface (Fig. 3, shaded areas). The 3- to 4-mm depth was suggested by results of preliminary studies. TI, TE, and PNG were continuously monitored online with a PowerLab system (*ADInstruments, Castle Hill, Australia; 16SP and Chart v5.5.6*). Average values of these variables and f_B were obtained for off-line analysis from data starting 2 min before and for the 10-min period after each DAMGO microinjection. At the end of each experiment, bilateral microinjections (~1 μl) of fluorescent latex microspheres (*Lumafluor. com; Red Retrobeads, Raleigh, North Carolina, USA*), diluted to 5% of the supplied concentration, were used to mark the most sensitive areas for histology. The brain stems were removed postmortem and submersed in paraformaldehyde fixative (4%) for 1 week before being frozen and sectioned. Sequential sections (25 μm) were cut from 10 to 17 mm rostral to obex. Alternate sections were stained with neutral red for histological identification of nuclear groups and compared with unstained adjacent sections showing fluorescent beads.

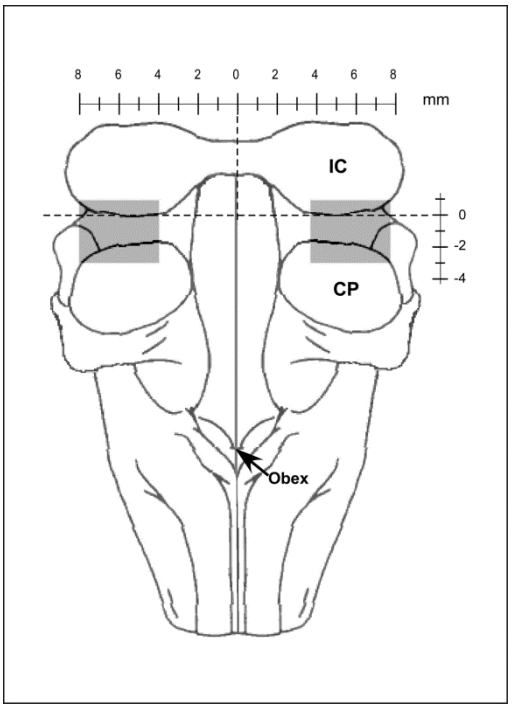

Figure 3. Schematic of the dorsal view of the canine pons/medulla with cerebellum removed showing the coordinate system used in this study. Shaded areas indicate the pontine region explored for opioid-induced bradypnea. The caudal pole of IC (inferior colliculi) and the midline were used as the R-C (rostral-caudal) and M-L (medial-lateral) initial (0/0) reference points, respectively. CP, cerebellar peduncle.

Protocol 2: Pontine microinjections of naloxone to reverse bradypnea induced by systemic remifentanil.

In a second series of animals (9 decerebrate and 12 anesthetized) after a control period of steady-state phrenic activity, remi was infused at an intravenous rate (0.1–1.0 $\mu g \cdot kg^{-1} \cdot min^{-1}$) to induce steady-state bradypnea (>60% decrease in central breathing frequency, f_B) or apnea. During continued steady-state remi infusion, a series of unilateral and bilateral microinjections of NAL (100 μM, ~550 nl each), within the opioid-sensitive pontine region delineated by the DAMGO protocol, were performed to localize the region in which it is possible to partially or totally antagonize the remi-induced bradypnea. Phrenic activity, TI, TE and the NAL microinjection marker signals were recorded with a PowerLab system. After successful antagonism by the NAL microinjections, the intravenous remi infusion was discontinued and PNG activity was followed until full recovery occurred. Repeat runs in the same animal to allow for complete mapping of opioid reversal of the region were separated by ~1 h to allow the microinjected NAL to diffuse out of the area. Microinjections of fluorescent beads were used to mark the most sensitive areas for histological purposes.

3.7. Data analysis

Protocol 1: Respiratory effects of direct pontine μOR activation via pontine microinjection of DAMGO.

The DAMGO microinjections resulted in a cumulative slowing of f_B in sensitive areas. Therefore the incremental effect of each additional microinjection off-line was calculated. A new local control was obtained from the data ~1 min prior to each microinjection. A second measurement was obtained 5–10 min after each microinjection but prior to the subsequent microinjection. These two values were used to calculate the percent change in f_B. To aid in this analysis, the breath-by-breath data were fitted via a regression procedure known as LOESS or LOWESS (88), in which a series of subsets of the data is used to provide the best fit that follows the trend features of the data. SigmaPlot 11 (*Systat Software, San Jose, CA, USA*) was used for this purpose and for plots used in the figures. Examples of the fits are indicated with red lines in the f_B data (BPM) in Fig. 4, A and B. Figure 4A shows an example of the effects of a series of DAMGO microinjections (vertical arrows) at the three locations indicated on breath-by-breath f_B (BPM) with the data fit superimposed (red line). Note the

cumulative effect of the microinjections on the slowing of phrenic respiratory rate. Time-expanded plots of the same data for each microinjection site are shown with time shifted relative to the time of microinjection in Fig. 4B (black arrowheads at microinjection, $t = 0$). From these plots, the incremental changes in f_B were calculated as a percent change from the preinjection local control values as indicated by arrows in Fig. 4B. Contour plots were constructed to display the percent change in f_B as a function of the location on the rostral-caudal (R-C) by medial-lateral (M-L) grid (Fig. 4A, bottom).

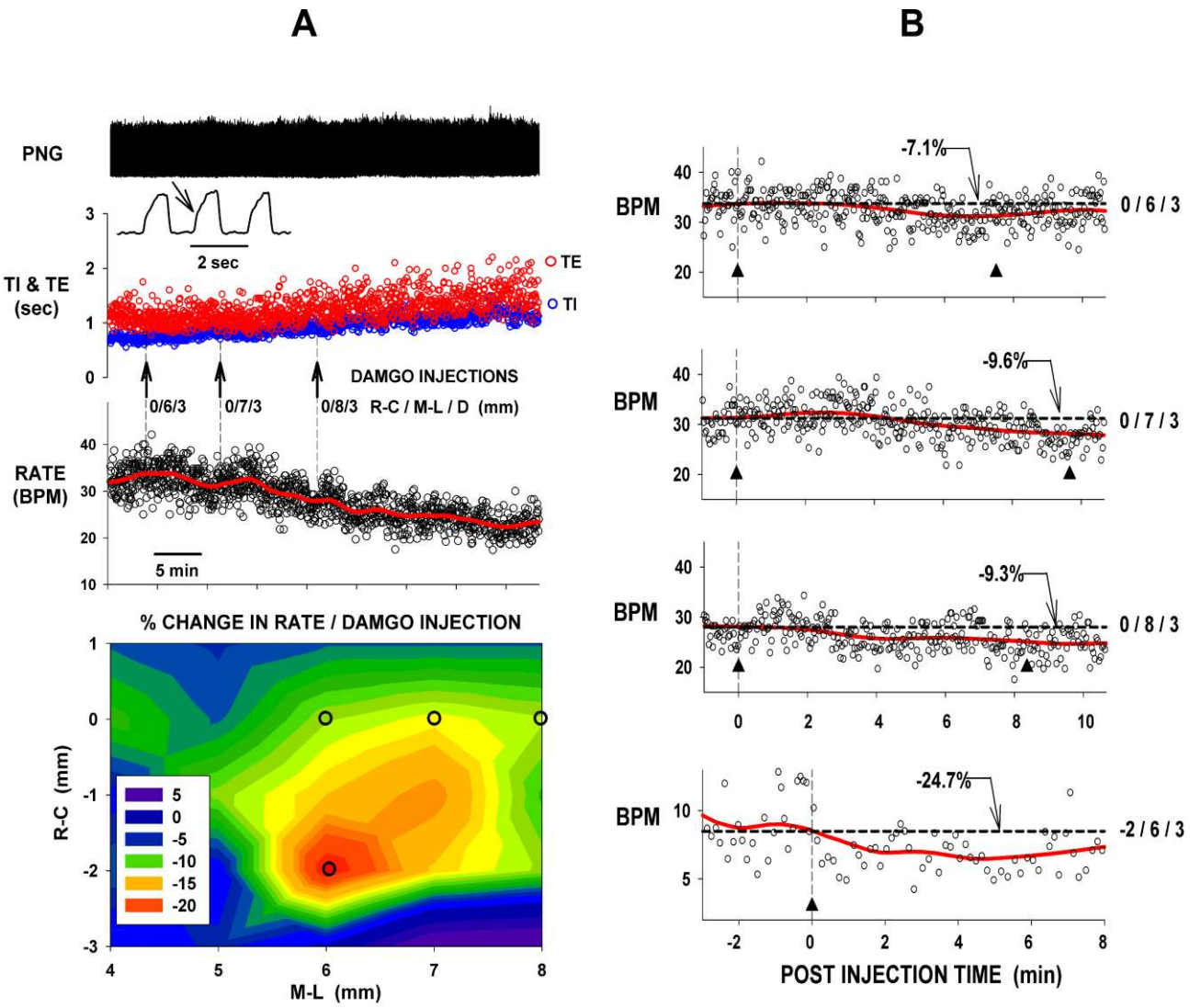

Figure 4. Example of data illustrating the methods used to quantify the effects of [D-Ala^2, N-Me-Phe^4,Gly-ol^5]-enkephalin (DAMGO) microinjections during the pontine mapping protocol (*protocol 1*). Microinjections of DAMGO (100 μM, 500 nl) were sequentially injected beginning at 0 rostral-caudal (R-C) and 4 lateral and progressed laterally until 8 mm lateral. The medial to lateral sequence of microinjections was subsequently repeated for -1, -2, -3 and +1 R-C. Typical depth of injections was 3 mm from dorsal surface (3rd coordinate). A, *top*: effects of a series of DAMGO microinjections [vertical arrows with coordinates as indicated: R-C/medial-lateral (M-L)/depth (D)] on the phrenic neurogram (PNG) and breath-by-breath values of TI (inspiratory time, blue symbols), TE (expiratory time, red symbols) and fictive breathing rate [f_B, breaths/min (BPM), black symbols]. The corresponding locations are shown by the 3 black circles at 0 R-C on the contour plot (*A, bottom*). Thick red line in rate data is the local regression curve (LOWESS function) indicating the best-fit trend.

Note that there is a progressive increase in TI and TE, a decrease in rate, and no change in peak PNG. B: time-expanded plots of f_B for the corresponding microinjections indicated on the contour plot (black circles) with time of injection set to 0 (vertical dashed lines). Red lines: best-fit regression curves. Because of cumulative effects of DAMGO, incremental % changes relative to the preinjection values (dashed horizontal lines) were calculated 6–10 min after injection (arrows with values). Arrowheads: time of microinjections. R-C, lateral, and depth coordinates are given at right of each plot. Contour plot (*A, bottom*) shows % reduction in breathing rate caused with DAMGO microinjections at the various R-C and M-L locations. In this example, the maximum change in f_B of ~25% occurred at -2 R-C and 6 lateral. Corresponding data are shown in *B, bottom*, with changed scale.

Protocol 2: Pontine microinjections of naloxone to reverse bradypnea induced by systemic remifentanil.

Breath-by-breath values of TI, TE, f_B and PPA were computed off-line continuously for the pre-remi baseline period, during intravenous remi infusion, and the post-remi infusion period. The LOWESS function was used to smooth the f_B data from which values were obtained to calculate the amount of remi-induced depression and the amount of reversal of that depression for each NAL microinjection. The following expressions were used to calculate the drug effects:

$$\% \text{ remi effect} = 100 \times (f_{remi} - f_{con}) / f_{con} \quad (1)$$

$$\% \text{ reversal (1st microinjection)} = 100 \times (f(1)_{NAL} - f_{remi}) / (f_{con} - f_{remi}) \quad (2)$$

$$\% \text{ reversal (}i\text{th microinjection)} = 100 \times (f(i+1)_{NAL} - f(i)_{NAL}) / (f_{con} - f_{remi}) \quad (3)$$

where f_{con} is pre-remi control f_B, f_{remi} is f_B during steady-state remi-induced bradypnea, $f(i)_{NAL}$ is the value of f_B 5–10 min after the ith NAL injection, and i designates the injection number within a sequence of microinjections during a remi protocol. The number of NAL injections is determined by the number required to obtain complete reversal of the remi effect.

3.8. Statistical Analyses

A one-way analysis of variance ANOVA was used to analyze changes in f_B due to microinjections at locations that were responsive to either DAMGO or NAL. The Holm-Sidak method was used for pairwise multiple comparisons with a family-wide error rate of 0.05. For all data sets, tests for normality (Kolmogorov-Smirnov test) were performed before parametric procedures were used. For data sets that failed the normality test, a Kruskal-Wallis one-way ANOVA on ranks was used with Dunn's method for multiple comparisons versus control group. Differences were considered significant at $P < 0.05$. Values are expressed as means ± standard error of the mean (SE).

4. RESULTS

Preliminary Study Findings

An example of the preliminary data showing the effects of 100 μM DAMGO applied to the dorsal surface of the pons between the IC and the superior cerebellar peduncle is shown in Fig. 5.

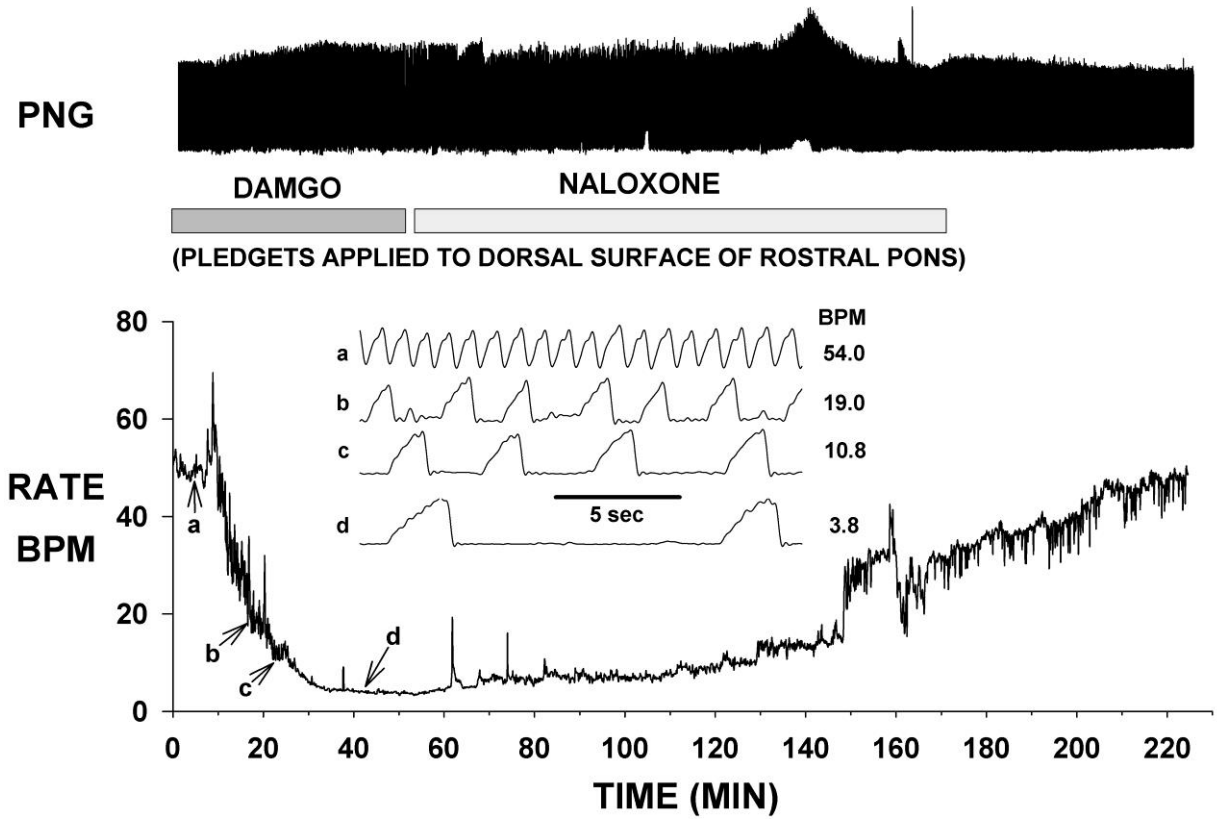

Figure 5. Preliminary data suggesting that μ-opioid receptors (MORs) in the dorsolateral pons may be the targets of systemically administered opioids that produce bradypnea at clinically relevant concentrations: example of the effects of DAMGO-saturated pledgets applied to the dorsal surface of the pons between the inferior colliculus (IC) and the superior cerebellar peduncle (SCP) of a dog on phrenic neurogram (PNG) and f_B. Note marked bradypnea and increases in TI and TE, with a small increase in peak PNG. Naloxone (NAL)-saturated pledgets gradually reversed the DAMGO-induced bradypnea.

The PNG burst rate decreased from ~54 BPM to ~4 BPM (~92% reduction). As TI increased, the peak PNG also increased slightly. At ~60 min into the protocol, the dorsal surface was rinsed with warm saline, and NAL (500 μM) pledgets, which were refreshed every ~6 min for an hour, were placed bilaterally to antagonize the DAMGO effects. This was followed by replacing the 500 μM NAL with 10 mM NAL to obtain a more complete reversal. For the preliminary group of animals, there was a 51 ± 15% reduction in PNG burst rate (n = 4) by the dorsal surface application of μ-opioids.

In addition, immunohistochemical mapping of MORs in one dog showed high levels of MOR-ir in the region of the lateral PBN (Fig. 6). Together, these findings led us to hypothesize that systemically administered μ-opioids produce bradypnea via MORs in the dorsolateral rostral pons.

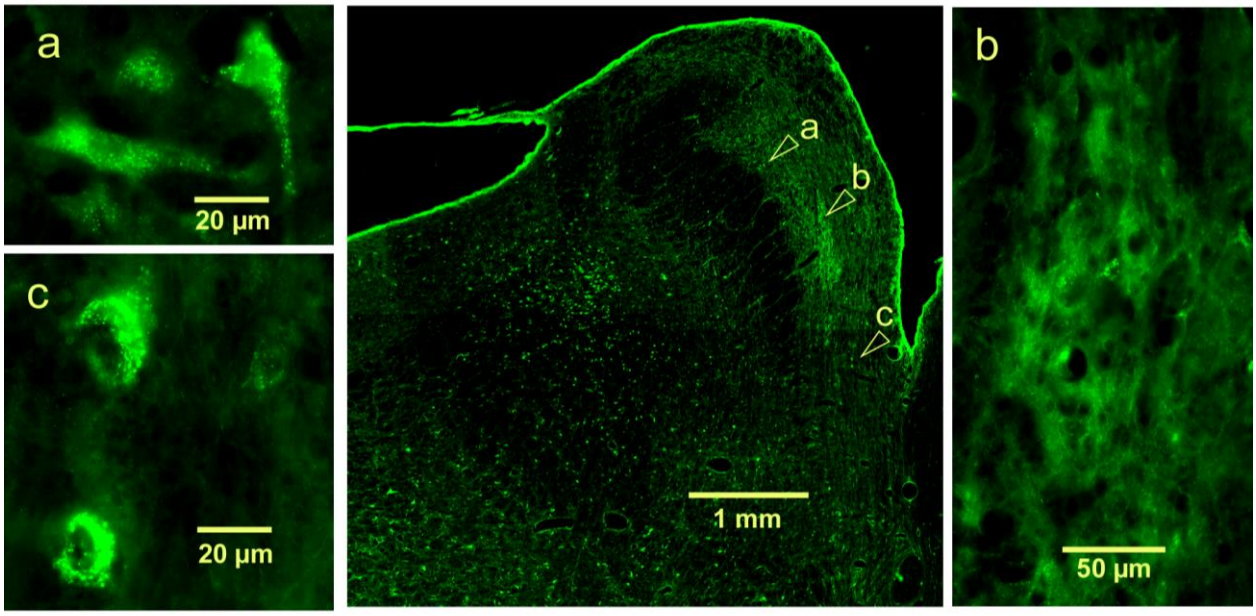

Figure 6. Distribution of µOR immunoreactivity (MOR-ir) in the rostral dorsal lateral pons showing the parabrachial/Kölliker-Fuse (PB-KF) complex. Center: fluorescence photomicrograph of a coronal section that shows a relatively high level of MOR-ir lateral to the superior cerebellar peduncle (arrowheads a–c) corresponding to the lateral PB complex. a and c: Higher-magnification images near arrowheads a and c show discrete points of high-density MOR-ir on cell somas. b: High level of MOR-ir of a filamentous network, possibly dendritic, near arrowheads b.

Protocol 1. Respiratory Effects of Direct Pontine μOR Activation via Pontine Microinjection of DAMGO

In 10 dogs, 286 DAMGO microinjections (390 ± 13 nl/microinjection; 28.6 ± 3.3 microinjections/dog) in the dorsal lateral pons extending from 1 mm rostral to the caudal pole of the IC to 3 mm caudal and from 4 to 8 mm lateral of the midline (shaded areas in Fig. 3) were performed to delineate the region that mediates an opioid induced decrease in f_B. Figure 7 shows an example of a series of unilateral DAMGO (100 μM, 500 nl each) microinjections in the lateral direction, which resulted in significant slowing from ~11 BPM to apnea (Fig. 7, bottom, f_B). The ~10-min apnea was subsequently reversed by intravenous NAL (~1 μg/kg; Fig. 7, right). PPA increased with the increase in TI.

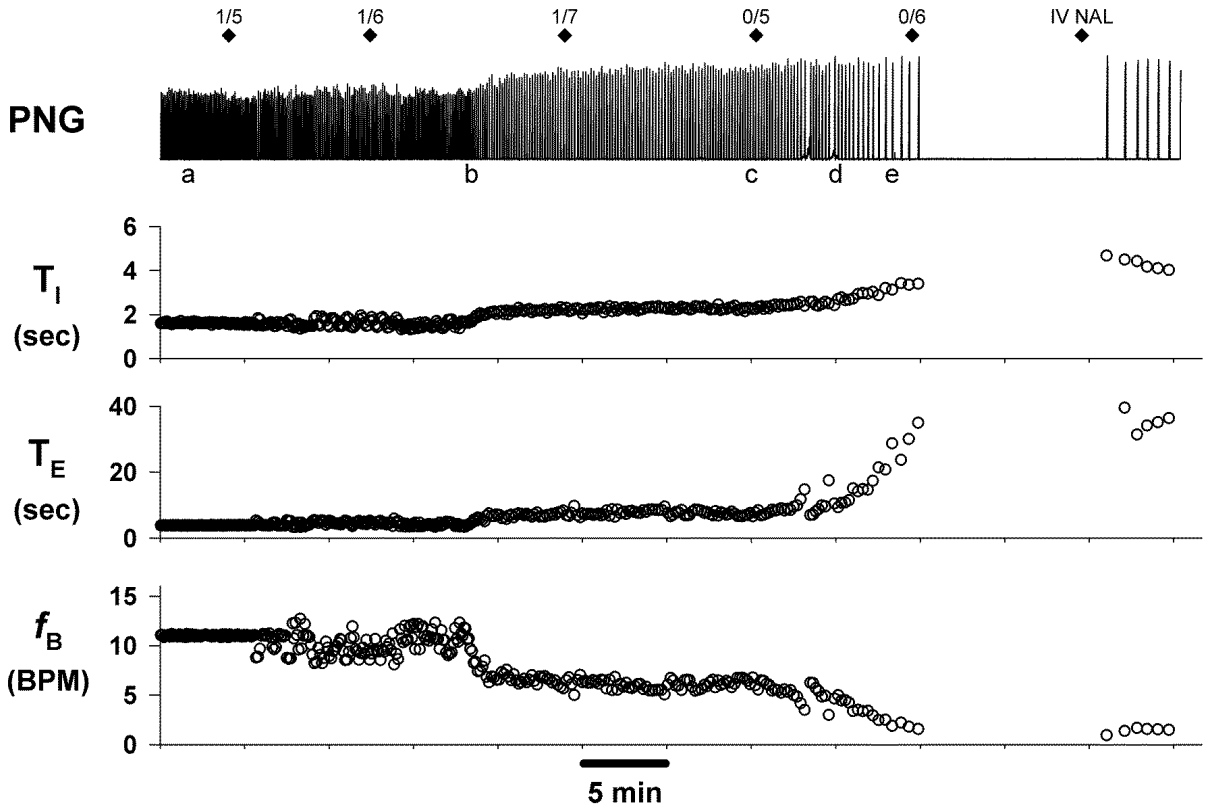

Figure 7. Example of the effects of a series of unilateral DAMGO microinjections (diamond symbols with pontine R-C/lateral coordinates). Note the progressive increases in TI (inspiratory time) and TE (expiratory time) and decrease in f_B and subsequent apnea. An IV bolus of naloxone (NAL, 10 μg/kg) partially antagonized the apnea. Larger subsequent doses were required to fully antagonize the DAMGO effects. A moderate increase in peak phrenic neurogram (PNG) is entirely due to the increase in TI without changes in drive (see Fig. 8 and text for further explanation).

Time-expanded records of PNG (Fig. 7, top) are shown in Fig. 8A and superimposed traces of the first cycle in each record in Fig. 8B. Note that the ramp slope of the PNG is not altered and the peak height is dependent on magnitude of TI, suggesting that respiratory drive has not changed. A nonlinear relationship between TI and the following TE of each cycle is also seen after vagotomy (Fig. 8C). While DAMGO increases both TI and TE, the major decrease in f_B is primarily due to the increase in TE.

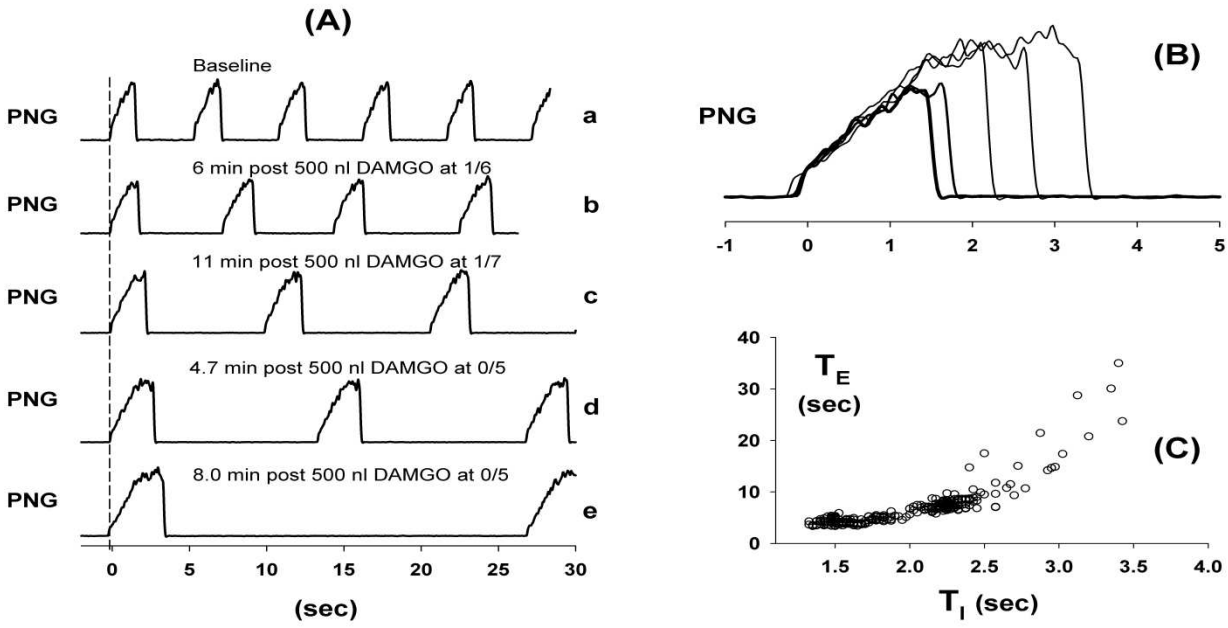

Figure 8. Pontine DAMGO microinjections produce changes in timing but not drive. A: time-expanded segments of phrenic neurogram (PNG) record in Fig. 7, top, at the times indicated (a–e) below the PNG trace. The 1st PNG cycle in each segment has been time aligned at 0 s. B: superimposed traces of the 1st breath cycle in each record. Note that the slope of the PNG ramp is not altered and the peak height is dependent on magnitude of TI, suggesting that respiratory drive has not changed. C: plot of TI vs. the subsequent TE of each cycle during vagotomy appears to be nonlinear. While DAMGO caused increases in both TI and TE, the large decreases in f_B are mainly due to the large increases in TE.

The data of the contour plots from 10 dogs were averaged at each of the grid coordinates to produce the contour plot of the average responses (Fig. 9).

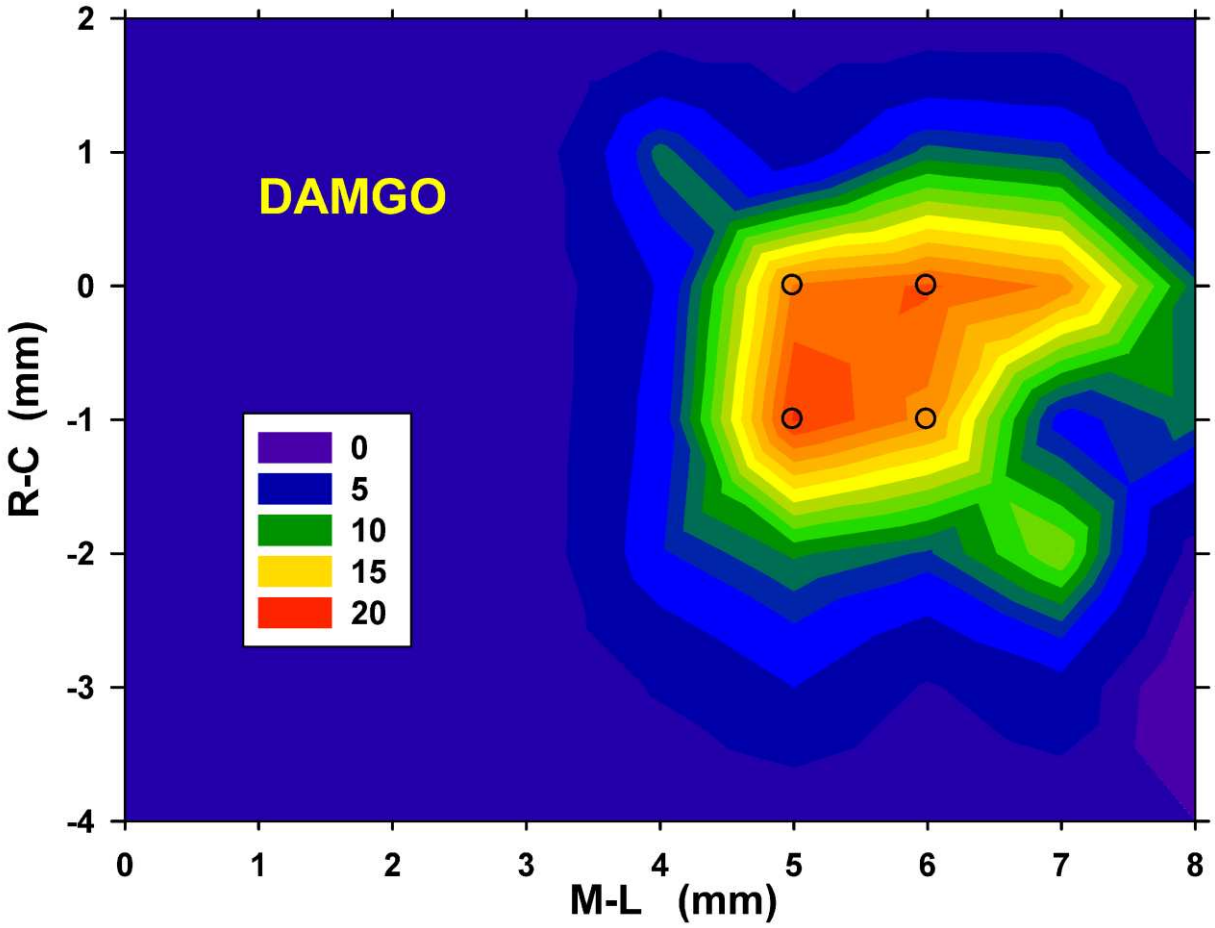

Figure 9. Contour plot for DAMGO-induced decreases in breathing frequency based on mean % change in breathing frequency (f_B) values obtained in 10 dogs. The most opioid responsive region was confined to an area of <2 x 2 mm. The largest decreases in f_B at any injection site were ~20% and were located at -1 R-C and 5 lateral. Superimposed open circles indicate sites from which data were tested for statistical significance (see text for details) (Fig. 10A).

The average magnitude of the incremental responses in f_B for the most sensitive locations, indicated by superimposed open circles in Fig. 9, top, are shown in Fig. 10A. The largest incremental responses were located at 5 to 6 mm lateral to midline and 0 to -1 caudal to the IC and were in the range of 15–20%. The cumulative maximum effect of a series of DAMGO microinjections per experiment was on average a 74 ± 6% reduction in baseline f_B from 18.6 ± 4.2 to 5.0 ± 1.5 BPM with 8.2 ± 1.1 microinjections. PPA was not significantly changed (0.78 ± 1.52%, n = 74 microinjections) by the DAMGO microinjections. The prominent and most consistent response over the lateral range of 4 to 8 mm from the midline was a >5% decrease in f_B as shown by the pooled response data from all R-C sites corresponding to each lateral site (Fig. 10B, Bradypnea). At some of the sites in some animals, DAMGO microinjections caused no response or an increase in f_B. However, increases in f_B >5% were seldom seen at 5–7 mm lateral (Fig. 10B, Tachypnea) and were observed less often than little or no responses (Fig. 10B, No Response).

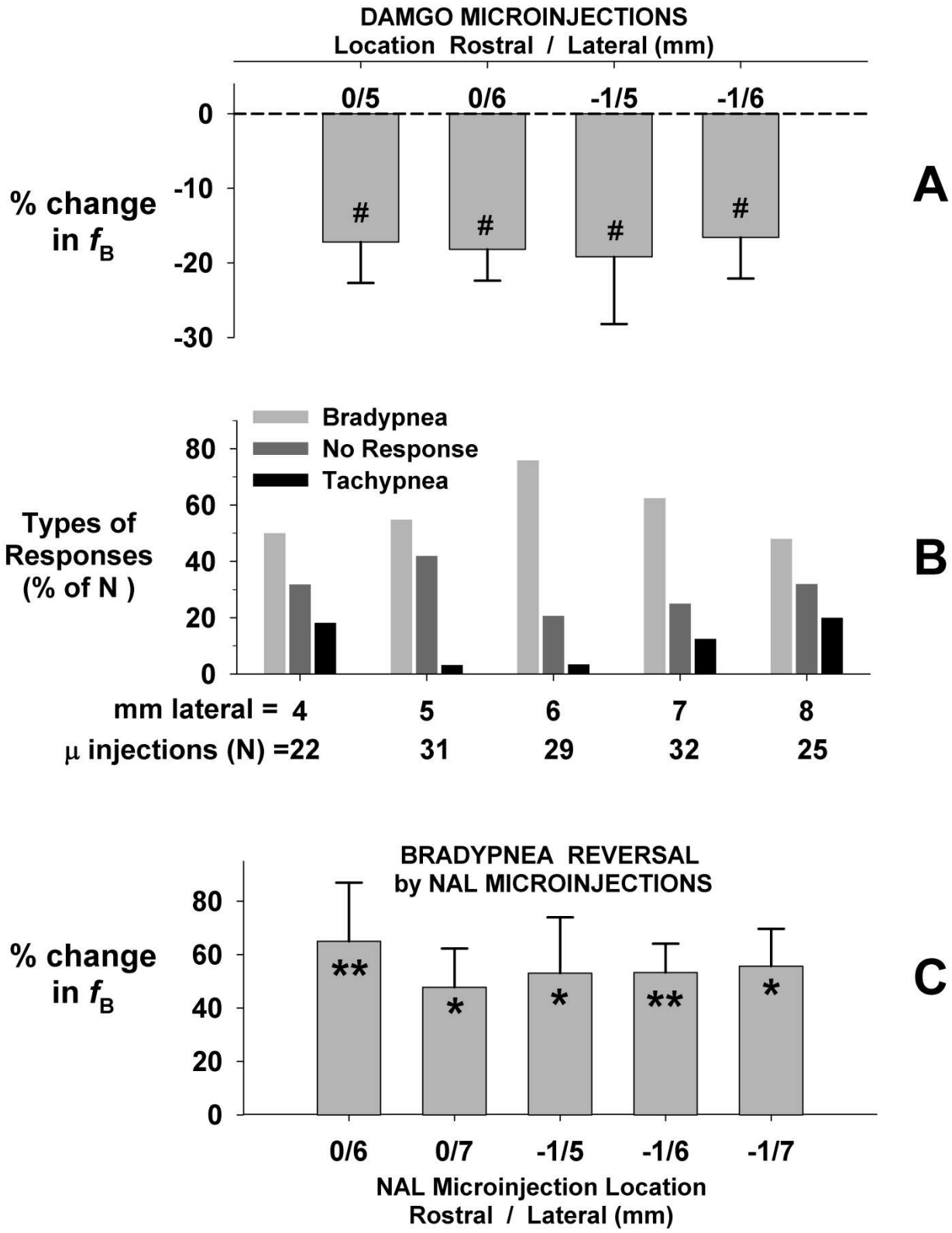

Figure 10. A: % change in f_B for each microinjection of 300–500 nl of 100 μM DAMGO at the site indicated above each bar (also in Fig. 9, open circles; n = 10 dogs). $^{\#}P < 0.05$ difference from zero change (1-way ANOVA). B: types of responses to DAMGO as % of the

number (N) of DAMGO microinjections per lateral coordinate (all R-C locations pooled). Tachypnea was rarely observed throughout the mapped region (darkest bars). C: % reversal of the remi-induced depression of f_B per NAL microinjection (540 nl of 100 μM NAL). *P < 0.05, **P < 0.01 changes relative to no effect (1-way ANOVA).

Protocol 2. Pontine Microinjections of Naloxone to Reverse Bradypnea Induced by Systemic Remifentanil

The reversal of remi-induced bradypnea by NAL microinjections in the region delineated by the DAMGO microinjections (*protocol 1*) was studied in 21 dogs. An example of a protocol is given in Fig. 11, where remi (0.8 $\mu g \cdot kg^{-1} \cdot min^{-1}$) markedly decreased the peak PNG and PNG ramp slope (not shown) and altered f_B.

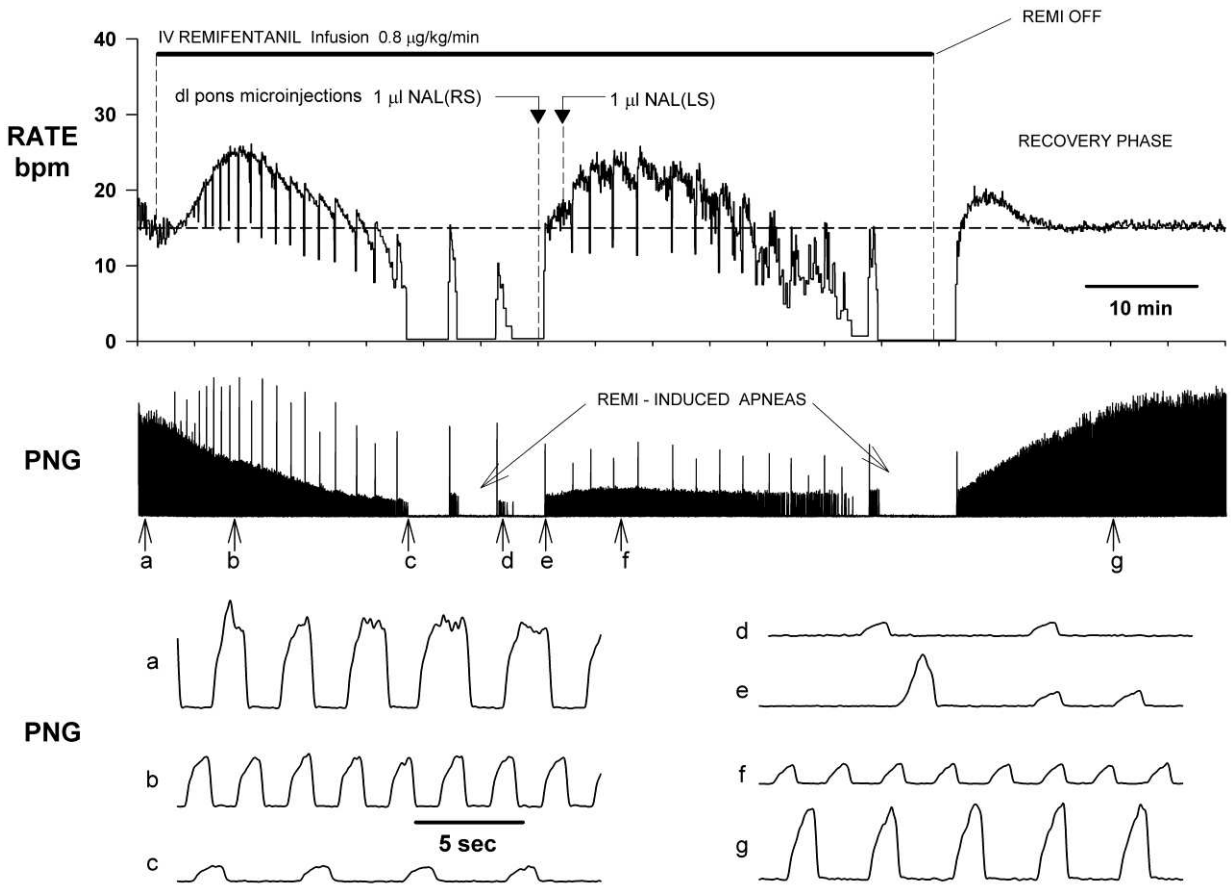

Figure 11. Example of the reversal of IV remi-induced bradypnea/apnea by NAL (100 μM) microinjections in the dorsolateral pons (-1 mm R-C, 7 mm lateral to midline, 3 mm ventral to dorsal surface). The IV remi infusion at a rate of 0.8 $\mu g \cdot kg^{-1} \cdot min^{-1}$ decreased peak PNG, PNG slope and breathing rate f_B until transient apneas ensued (PNG record, arrows). Intermittently, large sigh-like respiratory cycles were also observed. A transient increase in f_B above control baseline (RATE record, horizontal dashed line) was observed after initiation of remi infusion prior to bradypnea. Throughout the infusion, peak PNG gradually decreased until a steady-state plateau at ~20% peak PNG was reached. Peak PNG remained depressed after the two bilaterally symmetrical 1 μl NAL microinjections (compare records at times c, d, e, and f), while respiratory rate transiently recovered despite ongoing remi infusion. During the initial apneic period, short periods of phrenic activity reappeared (between times c and e), suggesting that the opioid plasma concentration was close to the phrenic apneic threshold. After 10 min of apnea, the first unilateral NAL microinjection reversed the apnea (the 2nd contralateral microinjection given as part of the protocol), and a transient tachypnea similar to

the initial one resulted without any notable change in peak PNG. As the effect of the bilaterally microinjected NAL gradually declined during sustained IV remi infusion, bradypnea and apnea eventually reoccurred. After termination of the remi infusion, both peak PNG and f_B gradually returned to pre-remi levels. The entire protocol lasted almost 2 h. Time-expanded records of PNG are shown for times indicated by the labeled arrows (a–g). e: Onset of reversal of the apnea by the 1st NAL microinjection, where the 1st PNG cycle shows a sigh in this case. At the end are shown time expanded traces with letters.

As illustrated in this example, after initiation of the remi infusion a transient increase in respiratory rate (tachypnea) was frequently observed (e.g., f_B above the dashed horizontal line, Fig. 11). This was followed by bradypnea and finally apnea as the remi infusion continued. Throughout this time, PPA gradually decreased until it reached a plateau well above zero (see PNG record before start of NAL microinjections and after, and time-expanded records c–f, Fig. 11). This suggests that the apnea resulted from an interruption of respiratory rhythm rather than completely suppressed peak PNG amplitude. The intermittent large tidal breaths illustrated in the peak PNGs are sigh-like cycles that are also frequently observed during remi infusions. During the apneic period, short periods of phrenic activity reappeared, suggesting that the selected remi infusion rate did not depress respiratory activity much below the phrenic apneic threshold. After ~10 min of apnea, bilateral pontine microinjections of NAL (1 μl each) were made at 7 mm lateral to the midline and 1 mm caudal to the caudal pole of the IC at a depth of ~3 mm, which completely reversed the apnea and resulted in a transient respiratory rate above the pre-remi control frequency (transient tachypnea). In this example, the first NAL microinjection was sufficient to initiate the reversal of the apnea. Despite these profound effects of pontine NAL microinjections on f_B, there was very little effect on peak PNG (Fig. 11, middle section between the 2 arrows). As the NAL effect gradually declined during continued remi infusion, bradypnea and apnea reoccurred. After termination of the remi infusion, peak PNG and f_B gradually returned to pre-remi levels. The length of the entire protocol was almost 2 h. During 39 NAL microinjection protocols, the pre-remi f_B of 14.8 ± 1.6 BPM was reduced by 72 ± 4% by 0.41 ± 0.05 $\mu g \cdot kg^{-1} \cdot min^{-1}$ of intravenous remi. The level of remi-induced depression of f_B was similar in decerebrate (n = 18 runs) versus isoflurane-anesthetized (n = 21 runs) dogs (-64 ± 6% vs. -78. ± 3%). However, to obtain this same level of depression, decerebrate dogs required a ~35% higher remi infusion rate than anesthetized dogs (0.46 ± 0.04 vs. 0.34 ± 0.04 $\mu g \cdot min^{-1} \cdot kg^{-1}$; P = 0.029). Remi also reduced the peak PNG by 25.3 ± 3.6%. There was no significant correlation between the degree of remi-induced depression in peak PNG and f_B (r = -0.24; P = 0.14, Spearman rank order).

A total of 84 NAL microinjections (540 ± 35 nl each) in 21 dogs (decerebrate and anesthetized) were used to map the region where reversal of remi-induced bradypnea was observed (Fig. 12).

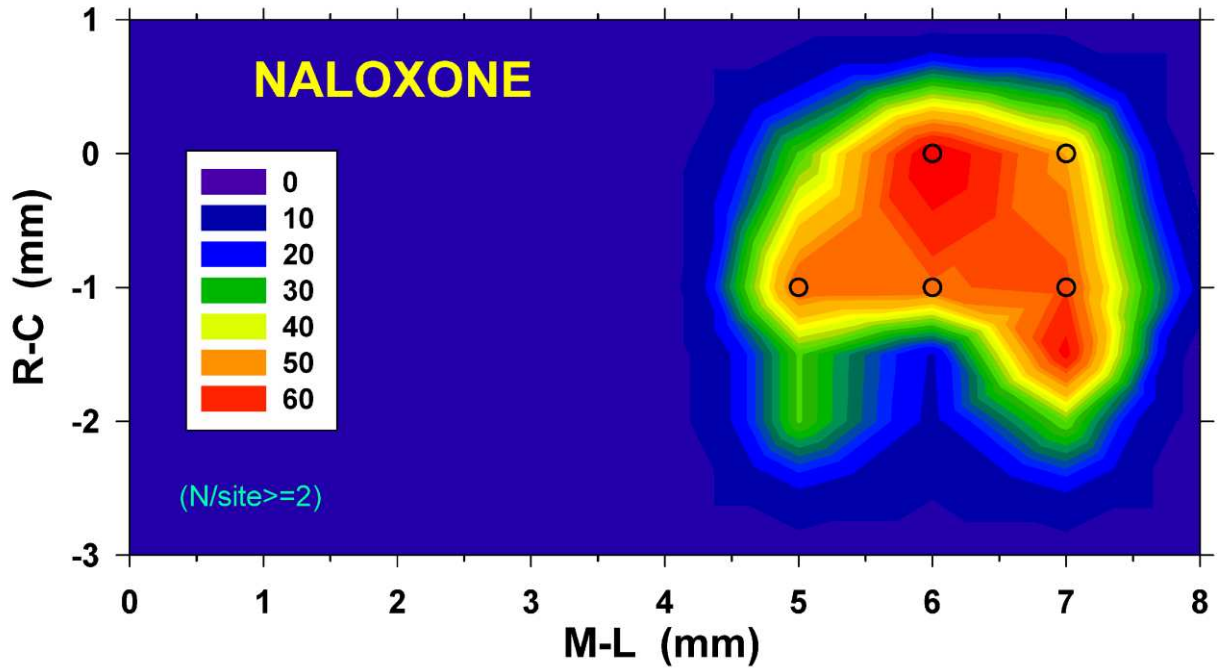

Figure 12. Contour plot for NAL (naloxone) microinjection reversal of IV remifentanil (remi)-induced bradypnea. Values are the average % of reversal of the maximum depression of f_B caused by remi from 21 dogs (see METHODS for more details regarding calculations). The largest mean values were ~60% (red). Open circles indicate sites where data were statistically analyzed as shown in Fig. 10C.

The average magnitude of the pooled responses at the most sensitive NAL locations of Fig. 12 (open circles) are given in Fig. 10*C*. The magnitude of bradypnea reversal was ~50% per NAL microinjection, and typically two NAL microinjections in these locations were able to completely reverse remi-induced bradypnea or apnea (101.8 ± 11.3%). There was no difference in the amount of NAL-induced reversal of the remi effect between the two types of preparations (107 ± 9% vs. 82 ± 14%, respectively). A total of 59 of the 84 NAL microinjections were located within the sensitive region extending from 0 to -1 mm rostrally and from 5 to 7 mm laterally (Fig. 10*C*). Unilateral microinjections (28/59) were just as effective as the bilateral microinjections (31/59), 46.7 ± 9.5% vs. 49.8 ± 8.2% ($P = 0.60$) reversal/ microinjection. For 12 protocols in 9 of the dogs, only a single microinjection at the first site selected within the sensitive region was able to produce complete reversal. The NAL microinjections that reversed remi-induced bradypnea had no effect on peak PNG (0.75 ± 4.1% change; $P = 0.86$) and only a small increase (7.1 ± 2.5% change; $P = 0.02$) in PNG/TI (average slope of the PNG). Since the remi-induced bradypnea protocols take 1.5–2 h to complete and only a small number of NAL microinjections were required to totally reverse the bradypnea, the number of NAL microinjections per experiment was less than the number of DAMGO injections in *protocol 1*.

Histological Identification of Most Effective NAL Injection Sites

Microinjections of fluorescent beads at the end of an experiment were placed bilaterally in the NAL microinjection sites that had produced the largest responses in f_B. An example of the location of the fluorescence in the PB region of the dorsolateral pons is shown in Fig. 13, left; the open circle indicates the location of the tip of the electrode at the bottom of the track that has been filled by the beads (arrow) during injection. The diagram in Fig. 13, right, shows the most effective sites for NAL reversal of remi-induced bradypnea, where the asterisks indicate sites based on the histologically verified fluorescent bead microinjections and the open circles indicate sites based on stereotaxic coordinates relative to the midline and depth. NAL microinjections in and near the brachium pontis (Fig. 13, right, asterisks) resulted in nearly complete (78–100%) reversal of the remi-induced bradypnea. Both the histological and the stereotaxic data from the NAL microinjection protocol suggest that activation of MORs in the PB-KF complex at a depth of 3–4 mm ventral to the dorsal surface mediates the intravenous remi-induced bradypnea.

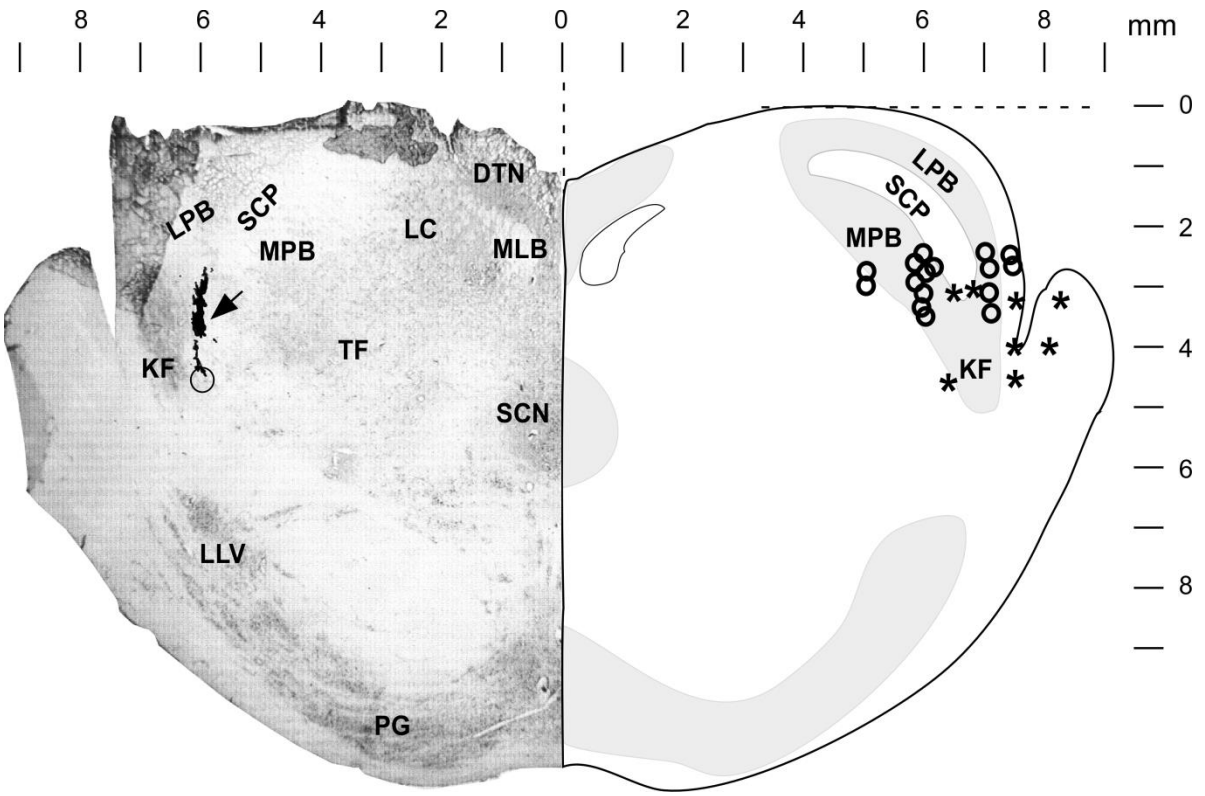

Figure 13. Left: section of rostral pons at the level of the caudal pole of the inferior colliculus (0 R-C) indicating the location of a microinjection in the most sensitive response area in this dog. The open circle indicates the location of the tip of the electrode at the bottom of the track (0 mm R-C, 6 mm lateral, 4.2 mm deep) that has been filled by the fluorescent beads (arrow) during injection and is just medial to KF. Right: diagram shows the most effective sites for NAL reversal of IV remi-induced bradypnea, where asterisks indicate sites based on the fluorescent bead microinjections and open circles indicate sites based on stereotaxic coordinates relative to the midline and depth for R-C coordinates from 0 to -2 mm relative to the caudal pole of the IC. NAL microinjections in and near the brachium pontis (lateral-most asterisks) resulted in nearly complete (78–100%) reversal of the remi-induced bradypnea, suggesting that MORs in the lateral parabrachial-KF complex mediate the remi-induced bradypnea. DTN, dorsal tegmental nucleus; KF, Kölliker-Fuse nucleus; LC, locus coeruleus; LLV, lateral lemniscus ventral nucleus; LPB, lateral parabrachial nucleus; MLB, medial longitudinal bundle; MPB, medial parabrachial nucleus; PG, pontine gray; SCN, superior central nucleus; SCP, superior cerebellar peduncle; TF, tegmental field.

5. DISCUSSION

This study shows that MORs in the pontine PB region play a key role in the control of breathing frequency in an adult in vivo preparation. In addition, this is the first study to show that MORs in this region are the primary targets where systemically administered MOR agonists produce bradypnea. Mapping with DAMGO microinjections delineated a 2 mm x 2 mm area, extending from 5 to 7 mm lateral of midline and from the caudal pole of the IC to 2 mm caudal of IC, in which it was possible to produce bradypnea in midcollicular decerebrate dogs. Within this same region, microinjections of NAL partially or totally reversed the depression of respiratory rate induced by intravenous remifentanil in a clinically analgesic dose range in both decerebrate and anesthetized dogs. In the DAMGO protocol, ~400 nl microinjections were made 1 mm apart in a grid-like manner. The estimated effective spherical radius of the microinjected drug, taking into account an extracellular volume fraction of 0.21 (89) and without subsequent diffusion (i.e., the initial volume), is ~750 μm. This provides overlapping volumes for microinjections spaced 1 mm apart. Since the brainstem with the cerebellum removed allowed direct visualization of the pons, stereotaxic measurements relative to the midline and caudal pole of the IC could be accurately and consistently made. Because DAMGO microinjections in this region produced a cumulative effect, it was necessary to estimate the incremental change in f_B for each subsequent microinjection as described in METHODS. The largest changes in f_B per microinjection ranged from 15% to 20% (Fig. 9 and Fig. 10A). Since PPA on average was not affected, we conclude that the MORs in this pontine region alter respiratory phase timing rather than respiratory drive, and this primarily by increases in TE (e.g., Figs. 4A, 7, and 8). We found that DAMGO microinjections did not reduce peak PNG; however, intravenous remifentanil reduced the peak PNG on average by 25.3 ± 3.6%. This suggests that remifentanil may have been acting at multiple sites within the respiratory control system, possibly in the ventral medulla as suggested by the study of Hurle et al. in spontaneously breathing, anesthetized cats (8).

The main objective of the second protocol was to determine whether the MORs that were activated by DAMGO and caused bradypnea in the first protocol were also responsible for the bradypnea produced by intravenous remifentanil at clinical tissue concentrations. Remifentanil was used in our study because of its rapid onset and short latency to peak effect, as well as its rapid recovery (context-sensitive half-life of ~4 min) (84), which is independent of dose rate and length of infusion and allowed us to perform multiple exposures in the same

experimental animal. The dose rate that abolishes reaction to surgical stimuli in 50% of patients was found to be ~0.5 $\mu g \cdot kg^{-1} \cdot min^{-1}$ and appears to be similar in dogs (86, 87). Larger microinjection volumes for NAL (540 ± 35 nl each), confined to the region delineated by the DAMGO protocol, reached a greater number of receptors per microinjection (effective spherical radius ~1 mm), achieving a larger reversal effect per injection (~50% reversal) and thus shortening each remi infusion protocol. Typically, two or three remifentanil infusion protocols with stable fictive breathing patterns were possible per experiment. Interestingly, symmetrical bilateral microinjections were no more effective than unilateral microinjections, even though twice as much volume was injected. The reason for this was not clear.

Role of Pontine Parabrachial/Kölliker-Fuse Complex in Control of Breathing Frequency

The results of this study emphasize the powerful role that the pontine PB-KF complex plays in the control of phase timing and breathing frequency (e.g., Fig. 7). The range of f_B control is remarkable, since microinjected DAMGO was capable of producing significant bradypnea up to complete respiratory arrest through increases in TE. On the other hand, remifentanil-induced bradypnea of similar magnitude (~72% reduction in baseline f_B) could be fully reversed by the pontine NAL microinjections. The importance of the pontine PB-KF complex in the control of breathing has been known for some time. This area has been referred to as the "pneumotaxic center" or, more recently, the pontine respiratory group (PRG) (48, 90). PRG neurons project to the ventral respiratory group (80). Electrical stimulation or chemical stimulation with glutamate in the lateral PB complex in cats or rats predominantly evoked respiratory facilitation, while stimulation of the more ventrally located KF nucleus or medial PBN decreased respiratory rate (91-93). Song and Poon also showed that bilateral lesions of the lateral PBN resulted in significant bradypnea (increase in TE) under hyperoxia and in marked attenuation of the tachypneic response (decrease in TE) to hypoxia (94). In vitro voltage-clamp experiments in rat lateral PB neurons show that MOR agonists increase the potassium conductance of the membrane and inhibit the neurons through hyperpolarization (95). It is thus reasonable to deduce that the inhibition of neurons whose excitation results in tachypnea would cause bradypnea. The maximum responses to DAMGO and NAL microinjections were located 5–7 mm lateral from midline, 0–1 mm caudal of the inferior colliculi, and 3–4 mm deep and correspond histologically with the structures of the PBN. There were more tachypneic responses medial of this area, suggesting that DAMGO microinjections into the medial PBN may have inhibited neurons that produce bradypnea

(93). Still, in a few animals DAMGO microinjections into the presumed lateral PBN had no effect or resulted in tachypnea (Fig. 10B), possibly due to anatomical differences among animals. The fact that complete reversals of bradypnea by single NAL microinjections were seen in the most lateral locations (i.e., 7 mm lateral, Fig. 12; also example in Fig. 11) suggests that the lateral PB region may play a significant role in the bradypneic effect of clinically used MOR agonists. However, significant effects were also found at 6 mm lateral to midline, which appears to correspond with the medial PBN. Because of the size of the microinjections and the subsequent diffusion, our ability to resolve the location within the PB complex is limited.

Other Brain Stem Sites Possibly Involved with Opioid-Induced Respiratory Depression

In adult rats, small numbers of weakly MOR-ir neurons and more abundant MOR-ir fibers and terminals were found throughout the rostrocaudal extent of the VRG (76). Interestingly, there appeared to be no difference in the number of MOR-ir neurons in the preBC compared with the BC complex. Other respiratory-related areas with intense MOR-like immunoreactivity were the pontine lateral PBN, the locus coeruleus, the rostral ambiguus nucleus, and the medial and commissural subnuclei of the NTS (80, 81). The mere presence of MORs, however, does not allow any conclusions as to their clinical significance. Similarly, the presence of μ- and δ-opioid receptors on canine respiratory premotor neurons in the VRC, demonstrated by picoejection of the respective agonist onto single neurons, did not translate into a depression of these neurons by clinical concentrations of a MOR agonist (75). The apparent reason was that the concentrations required for neuronal depression were in the 100–1,000 μM range with a threshold of 10 μM for morphine (75). Perhaps the concentration of synaptically released endogenous opioids is high enough to be effective on these neurons. In contrast, the plasma concentration of remifentanil in dogs at the infusion rate used in the present study (~0.5 $\mu g \cdot kg^{-1} \cdot min^{-1}$) is estimated to be ~14 nM (87), and the effect site concentration (extracellular fluid) may be ~50% lower (96). In whole brain tissue, the binding affinity for remifentanil was found to be 21.1 nM (97).

NAL microinjections did not always achieve a full reversal of the remi effect. Although this could be due to the spread of the drug within the PBN, it is possible that other areas of the brain stem may also contribute, to a lesser degree, to the opioid-induced respiratory depression. With microdialysis of fentanyl (100 μM) into the preBC region of anesthetized spontaneously breathing adult rats, it was reported that the preBC was solely responsible for

the respiratory rate suppression by systemic opioids (77). However, this study used relatively large, stereotaxically guided (relative to bregma) microdialysis probes (0.24-mm diameter, 1-mm length of permeable membrane) located at an average distance of 760 μm from the preBC (n = 8; based on corrected vector differences from Supplemental Table 1 in (77)). Since the respiratory effect was measured after dialyzing 100 μM fentanyl over 30–60 min, it is very difficult to judge the amount of fentanyl released or its concentration distribution within the brainstem. For example, genioglossus muscle activity was significantly depressed, even though the presumed location of hypoglossal premotor neurons was on average twice as far from the dialysis probes as the preBC (Supplemental Table 1 in (77)). The effective concentration of fentanyl in the brainstem most likely exceeded by far the plasma concentration of ~24 nM, which has been shown to depress minute ventilation by 57% in awake adult rats (98). Montandon et al. (2011) used an indirect method based on probe locations and response latencies to estimate the site of respiratory depression. However, because of the heterogeneity of brain tissue, the rate of diffusion will vary with path direction, as shown in their data by comparing diffusion-front velocities (distance/latency; Supplemental Table 1 in (77)), and result in dubious estimates of effect-site locations. Other *in vivo* studies suggest that the preBC is not the location of opioid-induced respiratory depression. Unilateral microinjection of the potent endogenous MOR agonist endomorphin-1 (60 nl, 10 mM, binding affinity Ki: 0.36 nM; (99)) into both the preBC and BC complex in adult rats produced an increase in phrenic burst rate, rather than a bradypneic response that is observed clinically (76). These findings are consistent with those in decerebrate dogs, where localized microinjections of DAMGO (~140 nl, 100 μM) within the functionally identified preBC region produced tachypnea (44% increase in f_B; n = 16), while intravenous infusion of remifentanil counteracted the DAMGO-induced tachypnea and produced marked bradypnea (55% decrease in f_B relative to baseline control) (2). More importantly, multiple bilateral microinjections of NAL (500 μM, 120 nl each, 3 per side) into the preBC region during steady-state remifentanil-induced bradypnea had no effect on f_B and PPA (2). Finally, in awake goats, relatively large microinjections (10 μl) of DAMGO (100 nM) into the preBC had no effect on the eupneic breathing pattern (100). Altogether, these studies suggest that the preBC is not directly involved in decrease in respiratory rate by clinical concentrations of opioids. Because of the invasive nature of our studies that require anesthesia, it is not possible to assess the opioid-induced effects on breathing in the cortex and other supra-brain stem structures, which may play an important role in the awake state. For example, Pattinson et al.

(2009), using MRI studies in awake volunteers, showed that remifentanil reduced the urge to breathe and this was associated with a decrease in activity in the left anterior insula and operculum cortical areas (101). However, our studies were focused on the effects of opioids on the automatic control of breathing, where opioids cause dose-dependent bradypnea.

6. CONCLUSIONS

This study has shown that microinjections of DAMGO in the region of the PBN cause significant decreases in f_B and microinjections of NAL in the same PB region completely reverse the bradypnea induced by systemically administered opioids at concentrations clinically relevant for analgesia.

Thus it appears that the PB complex, which is a major relay center for converging visceral, nociceptive, and thermoreceptive information to the forebrain (102-104), is a major site of opioid-induced respiratory depression.

Pontine PB-KF complex plays the powerful role in the control of phase timing and breathing frequency.

7. SUMMARY

AIM: Systemic administration of μ-opioids at clinical doses for analgesia decreases respiratory rate. MORs (μ-opioid receptors) within the PB (parabrachial) complex are potential targets. The purpose of this study was to define the pontine region in which MOR agonists produce bradypnea and to determine whether antagonism of MORs in this region reverses the bradypnea produced by systemic administration of clinically relevant concentrations of the MOR agonist remifentanil.

METHODS: The effects of microinjections of agonist [D-Ala2, N-Me-Phe4, Gly-ol5]-enkephalin (DAMGO; 100 μM) and antagonist naloxone (NAL; 100 μM) into the dorsal rostral pons on the phrenic neurogram were studied in a decerebrate, vagotomized, ventilated, paralyzed canine preparation during hyperoxia. A 1-mm grid pattern of microinjections was used. The DAMGO-sensitive region extended from 5 to 7 mm lateral of midline and from 0 to 2 mm caudal of the inferior colliculus at a depth of 3–4 mm. Inspiratory and expiratory durations (T_I and T_E) and peak phrenic nerve activity (PPA) were measured from the phrenic neurogram.

RESULTS: Microinjections of DAMGO in the region of the PBN (parabrachial nuclei) cause significant decreases in f_B and microinjections of NAL in the same PB region completely reverse the bradypnea induced by systemically administered opioids at concentrations clinically relevant for analgesia.

CONCLUSION: These results indicate that PB complex, which is a major relay center for converging visceral, nociceptive, and thermoreceptive information to the forebrain is a major site of opioid-induced respiratory depression. This study emphasizes the powerful role that the pontine PB-KF complex (parabrachial/Kölliker-Fuse) plays in the control of phase timing and breathing frequency.

8. REFERENCES

1. Gray PA, Rekling JC, Bocchiaro CM, Feldman JL. Modulation of respiratory frequency by peptidergic input to rhythmogenic neurons in the preBotzinger complex. Science 1999;286:1566-8.
2. Mustapic S, Radocaj T, Sanchez A, et al. Clinically relevant infusion rates of mu-opioid agonist remifentanil cause bradypnea in decerebrate dogs but not via direct effects in the pre-Botzinger complex region. J Neurophysiol 2010;103:409-18.
3. Haji A, Yamazaki H, Ohi Y, Takeda R. Distribution of mu receptors in the ventral respiratory group neurons; immunohistochemical and pharmacological studies in decerebrate cats. Neurosci Lett 2003;351:37-40.
4. Janczewski WA, Onimaru H, Homma I, Feldman JL. Opioid-resistant respiratory pathway from the preinspiratory neurones to abdominal muscles: in vivo and in vitro study in the newborn rat. J Physiol 2002;545:1017-26.
5. Mansour A, Fox CA, Burke S, Akil H, Watson SJ. Immunohistochemical localization of the cloned mu opioid receptor in the rat CNS. J Chem Neuroanat 1995;8:283-305.
6. Martin-Schild S, Gerall AA, Kastin AJ, Zadina JE. Differential distribution of endomorphin 1- and endomorphin 2-like immunoreactivities in the CNS of the rodent. J Comp Neurol 1999;405:450-71.
7. Sales N, Riche D, Roques BP, Denavit-Saubie M. Localization of mu- and delta-opioid receptors in cat respiratory areas: an autoradiographic study. Brain Res 1985;344:382-6.
8. Hurle MA, Mediavilla A, Florez J. Differential respiratory patterns induced by opioids applied to the ventral medullary and dorsal pontine surfaces of cats. Neuropharmacology 1985;24:597-606.
9. Feldman JL, Del Negro CA, Gray PA. Understanding the rhythm of breathing: so near, yet so far. Annu Rev Physiol 2013;75:423-52.
10. Lalley PM. Opioidergic and dopaminergic modulation of respiration. Respir Physiol Neurobiol 2008;164:160-7.
11. Feldman JL MD. Neuronal Control of Breathing. Fundamental Neuroscience. Third Edition ed: Elsevier Inc.; 2008. p. 855-72.
12. Ramirez JM, Anderson TM, Garcia AJ, 3rd. The ins and outs of breathing. Elife 2014;3:e03375.
13. Alheid GF, McCrimmon DR. The chemical neuroanatomy of breathing. Respir Physiol Neurobiol 2008;164:3-11.
14. Richter DW, Smith JC. Respiratory rhythm generation in vivo. Physiology (Bethesda) 2014;29:58-71.
15. Saether K, Hilaire G, Monteau R. Dorsal and ventral respiratory groups of neurons in the medulla of the rat. Brain Res 1987;419:87-96.

16. Kubin L, Alheid GF, Zuperku EJ, McCrimmon DR. Central pathways of pulmonary and lower airway vagal afferents. J Appl Physiol (1985) 2006;101:618-27.
17. Gestreau C, Milano S, Bianchi AL, Grelot L. Activity of dorsal respiratory group inspiratory neurons during laryngeal-induced fictive coughing and swallowing in decerebrate cats. Exp Brain Res 1996;108:247-56.
18. Stornetta RL. Identification of neurotransmitters and co-localization of transmitters in brainstem respiratory neurons. Respir Physiol Neurobiol 2008;164:18-27.
19. Feldman JL, Del Negro CA. Looking for inspiration: new perspectives on respiratory rhythm. Nat Rev Neurosci 2006;7:232-42.
20. Onimaru H, Homma I. A novel functional neuron group for respiratory rhythm generation in the ventral medulla. J Neurosci 2003;23:1478-86.
21. Stornetta RL, Sevigny CP, Guyenet PG. Inspiratory augmenting bulbospinal neurons express both glutamatergic and enkephalinergic phenotypes. J Comp Neurol 2003;455:113-24.
22. Dobbins EG, Feldman JL. Brainstem network controlling descending drive to phrenic motoneurons in rat. J Comp Neurol 1994;347:64-86.
23. Guyenet PG, Sevigny CP, Weston MC, Stornetta RL. Neurokinin-1 receptor-expressing cells of the ventral respiratory group are functionally heterogeneous and predominantly glutamatergic. J Neurosci 2002;22:3806-16.
24. Smith JC, Ellenberger HH, Ballanyi K, Richter DW, Feldman JL. Pre-Botzinger complex: a brainstem region that may generate respiratory rhythm in mammals. Science 1991;254:726-9.
25. Gray PA, Hayes JA, Ling GY, et al. Developmental origin of preBotzinger complex respiratory neurons. J Neurosci 2010;30:14883-95.
26. Janczewski WA, Feldman JL. Distinct rhythm generators for inspiration and expiration in the juvenile rat. J Physiol 2006;570:407-20.
27. Guyenet PG, Wang H. Pre-Botzinger neurons with preinspiratory discharges "in vivo" express NK1 receptors in the rat. J Neurophysiol 2001;86:438-46.
28. Lieske SP, Thoby-Brisson M, Telgkamp P, Ramirez JM. Reconfiguration of the neural network controlling multiple breathing patterns: eupnea, sighs and gasps [see comment]. Nat Neurosci 2000;3:600-7.
29. Butera RJ, Jr., Rinzel J, Smith JC. Models of respiratory rhythm generation in the pre-Botzinger complex. I. Bursting pacemaker neurons. J Neurophysiol 1999;82:382-97.
30. Del Negro CA, Koshiya N, Butera RJ, Jr., Smith JC. Persistent sodium current, membrane properties and bursting behavior of pre-botzinger complex inspiratory neurons in vitro. J Neurophysiol 2002;88:2242-50.
31. Koizumi H, Smith JC. Persistent Na+ and K+-dominated leak currents contribute to respiratory rhythm generation in the pre-Botzinger complex in vitro. J Neurosci 2008;28:1773-85.

32. Del Negro CA, Hayes JA, Pace RW, Brush BR, Teruyama R, Feldman JL. Synaptically activated burst-generating conductances may underlie a group-pacemaker mechanism for respiratory rhythm generation in mammals. Prog Brain Res 2010;187:111-36.
33. Johnson SM, Smith JC, Funk GD, Feldman JL. Pacemaker behavior of respiratory neurons in medullary slices from neonatal rat. J Neurophysiol 1994;72:2598-608.
34. Thoby-Brisson M, Ramirez JM. Identification of two types of inspiratory pacemaker neurons in the isolated respiratory neural network of mice. J Neurophysiol 2001;86:104-12.
35. Del Negro CA, Morgado-Valle C, Hayes JA, et al. Sodium and calcium current-mediated pacemaker neurons and respiratory rhythm generation. J Neurosci 2005;25:446-53.
36. Doi A, Ramirez JM. Neuromodulation and the orchestration of the respiratory rhythm. Respir Physiol Neurobiol 2008;164:96-104.
37. Smith JC, Abdala AP, Rybak IA, Paton JF. Structural and functional architecture of respiratory networks in the mammalian brainstem. Philos Trans R Soc Lond B Biol Sci 2009;364:2577-87.
38. Molkov YI, Abdala AP, Bacak BJ, Smith JC, Paton JF, Rybak IA. Late-expiratory activity: emergence and interactions with the respiratory CpG. J Neurophysiol;104:2713-29.
39. Rubin JE, Shevtsova NA, Ermentrout GB, Smith JC, Rybak IA. Multiple rhythmic states in a model of the respiratory central pattern generator. J Neurophysiol 2009;101:2146-65.
40. Smith JC, Abdala AP, Koizumi H, Rybak IA, Paton JF. Spatial and functional architecture of the mammalian brain stem respiratory network: a hierarchy of three oscillatory mechanisms. J Neurophysiol 2007;98:3370-87.
41. Liu YY, Wong-Riley MT, Liu JP, et al. Substance P and enkephalinergic synapses onto neurokinin-1 receptor-immunoreactive neurons in the pre-Botzinger complex of rats. Eur J Neurosci 2004;19:65-75.
42. Morgado-Valle C, Baca SM, Feldman JL. Glycinergic pacemaker neurons in preBotzinger complex of neonatal mouse. J Neurosci 2010;30:3634-9.
43. Pagliardini S, Adachi T, Ren J, Funk GD, Greer JJ. Fluorescent tagging of rhythmically active respiratory neurons within the pre-Botzinger complex of rat medullary slice preparations. J Neurosci 2005;25:2591-6.
44. Pena F, Ramirez JM. Substance P-mediated modulation of pacemaker properties in the mammalian respiratory network. J Neurosci 2004;24:7549-56.
45. Purvis LK, Smith JC, Koizumi H, Butera RJ. Intrinsic bursters increase the robustness of rhythm generation in an excitatory network. J Neurophysiol 2007;97:1515-26.
46. Manzke T, Guenther U, Ponimaskin EG, et al. 5-HT4(a) receptors avert opioid-induced breathing depression without loss of analgesia. Science 2003;301:226-9.

47. Tan W, Janczewski WA, Yang P, Shao XM, Callaway EM, Feldman JL. Silencing preBotzinger complex somatostatin-expressing neurons induces persistent apnea in awake rat. Nat Neurosci 2008;11:538-40.
48. Bianchi AL, Denavit-Saubie M, Champagnat J. Central control of breathing in mammals: neuronal circuitry, membrane properties, and neurotransmitters. Physiol Rev 1995;75:1-45.
49. Tan W, Pagliardini S, Yang P, Janczewski WA, Feldman JL. Projections of preBotzinger complex neurons in adult rats. J Comp Neurol 2010;518:1862-78.
50. Ezure K, Tanaka I, Kondo M. Glycine is used as a transmitter by decrementing expiratory neurons of the ventrolateral medulla in the rat. J Neurosci 2003;23:8941-8.
51. Krolo M, Stuth EA, Tonkovic-Capin M, Hopp FA, McCrimmon DR, Zuperku EJ. Relative magnitude of tonic and phasic synaptic excitation of medullary inspiratory neurons in dogs. Am J Physiol Regul Integr Comp Physiol 2000;279:R639-49.
52. Guyenet PG, Stornetta RL, Bayliss DA. Central respiratory chemoreception. J Comp Neurol 2010;518:3883-906.
53. Guyenet PG, Stornetta RL, Bayliss DA. Retrotrapezoid nucleus and central chemoreception. J Physiol 2008;586:2043-8.
54. Mulkey DK, Stornetta RL, Weston MC, et al. Respiratory control by ventral surface chemoreceptor neurons in rats. Nat Neurosci 2004;7:1360-9.
55. Takakura AC, Moreira TS, Stornetta RL, West GH, Gwilt JM, Guyenet PG. Selective lesion of retrotrapezoid Phox2b-expressing neurons raises the apnoeic threshold in rats. J Physiol 2008;586:2975-91.
56. Mellen NM, Janczewski WA, Bocchiaro CM, Feldman JL. Opioid-induced quantal slowing reveals dual networks for respiratory rhythm generation. Neuron 2003;37:821-6.
57. Segers LS, Nuding SC, Dick TE, et al. Functional connectivity in the pontomedullary respiratory network. J Neurophysiol 2008;100:1749-69.
58. Song G, Yu Y, Poon CS. Cytoarchitecture of pneumotaxic integration of respiratory and nonrespiratory information in the rat. J Neurosci 2006;26:300-10.
59. Ezure K, Tanaka I. Distribution and medullary projection of respiratory neurons in the dorsolateral pons of the rat. Neuroscience 2006;141:1011-23.
60. Zuperku EJ, Prkic I, Stucke AG, Miller JR, Hopp FA, Stuth EA. Automatic classification of canine PRG neuronal discharge patterns using K-means clustering. Respir Physiol Neurobiol 2014;207:28-39.
61. Alheid GF, Milsom WK, McCrimmon DR. Pontine influences on breathing: an overview. Respir Physiol Neurobiol 2004;143:105-14.

62. Dutschmann M, Herbert H. NMDA and GABAA receptors in the rat Kolliker-Fuse area control cardiorespiratory responses evoked by trigeminal ethmoidal nerve stimulation. J Physiol 1998;510 (Pt 3):793-804.
63. Stuth EAE SA, Zuperku EJ editor. Central effects of general anesthesia. 2008/08/30 ed: FL: Taylor and Francis; 2005.
64. St-John WM, Paton JF. Role of pontile mechanisms in the neurogenesis of eupnea. Respir Physiol Neurobiol 2004;143:321-32.
65. Lydic R, Orem J. Respiratory neurons of the pneumotaxic center during sleep and wakefulness. Neurosci Lett 1979;15:187-92.
66. Janecka A, Fichna J, Janecki T. Opioid receptors and their ligands. Curr Top Med Chem 2004;4:1-17.
67. Le Merrer J, Becker JA, Befort K, Kieffer BL. Reward processing by the opioid system in the brain. Physiol Rev 2009;89:1379-412.
68. Cashman JN, Dolin SJ. Respiratory and haemodynamic effects of acute postoperative pain management: evidence from published data. Br J Anaesth 2004;93:212-23.
69. Pattinson KT. Opioids and the control of respiration. Br J Anaesth 2008;100:747-58.
70. Law PY, Wong YH, Loh HH. Molecular mechanisms and regulation of opioid receptor signaling. Annu Rev Pharmacol Toxicol 2000;40:389-430.
71. Pert CB, Snyder SH. Opiate receptor: demonstration in nervous tissue. Science 1973;179:1011-4.
72. Wittert G, Hope P, Pyle D. Tissue distribution of opioid receptor gene expression in the rat. Biochem Biophys Res Commun 1996;218:877-81.
73. Pan HL, Wu ZZ, Zhou HY, Chen SR, Zhang HM, Li DP. Modulation of pain transmission by G-protein-coupled receptors. Pharmacol Ther 2008;117:141-61.
74. John McDonald DL. Opioid receptors. Continuing Education in Anaesthesia, Critical Care & Pain 2005;5.
75. Stucke AG, Zuperku EJ, Sanchez A, et al. Opioid receptors on bulbospinal respiratory neurons are not activated during neuronal depression by clinically relevant opioid concentrations. J Neurophysiol 2008;100:2878-88.
76. Lonergan T, Goodchild AK, Christie MJ, Pilowsky PM. Mu opioid receptors in rat ventral medulla: effects of endomorphin-1 on phrenic nerve activity. Respir Physiol Neurobiol 2003;138:165-78.
77. Montandon G, Qin W, Liu H, Ren J, Greer JJ, Horner RL. PreBotzinger complex neurokinin-1 receptor-expressing neurons mediate opioid-induced respiratory depression. J Neurosci 2011;31:1292-301.

78. Ren J, Ding X, Funk GD, Greer JJ. Ampakine CX717 protects against fentanyl-induced respiratory depression and lethal apnea in rats. Anesthesiology 2009;110:1364-70.
79. Glatzer NR, Smith BN. Modulation of synaptic transmission in the rat nucleus of the solitary tract by endomorphin-1. J Neurophysiol 2005;93:2530-40.
80. Chamberlin NL, Mansour A, Watson SJ, Saper CB. Localization of mu-opioid receptors on amygdaloid projection neurons in the parabrachial nucleus of the rat. Brain Res 1999;827:198-204.
81. Ding YQ, Kaneko T, Nomura S, Mizuno N. Immunohistochemical localization of mu-opioid receptors in the central nervous system of the rat. J Comp Neurol 1996;367:375-402.
82. Eguchi K, Tadaki E, Simbulan D, Jr., Kumazawa T. Respiratory depression caused by either morphine microinjection or repetitive electrical stimulation in the region of the nucleus parabrachialis of cats. Pflugers Arch 1987;409:367-73.
83. Tonkovic-Capin M, Krolo M, Stuth EA, Hopp FA, Zuperku EJ. Improved method of canine decerebration. J Appl Physiol (1985) 1998;85:747-50.
84. Burkle H, Dunbar S, Van Aken H. Remifentanil: a novel, short-acting, mu-opioid. Anesth Analg 1996;83:646-51.
85. Servin FS, Billard V. Remifentanil and other opioids. Handb Exp Pharmacol 2008:283-311.
86. Michelsen LG, Hug CC, Jr. The pharmacokinetics of remifentanil. J Clin Anesth 1996;8:679-82.
87. Michelsen LG, Salmenpera M, Hug CC, Jr., Szlam F, VanderMeer D. Anesthetic potency of remifentanil in dogs. Anesthesiology 1996;84:865-72.
88. Cleveland WS, Devlin S. J. . Locally weighted regression: an approach to regression analysis by local fitting J Am Stat Assoc 1988;83:596-610.
89. Nicholson C. Diffusion from an injected volume of a substance in brain tissue with arbitrary volume fraction and tortuosity. Brain Res 1985;333:325-9.
90. Feldman. Neurophysiology of breathing in mammals: Am Physiol Soc; 1986. 463–524 p.
91. Chamberlin NL, Saper CB. Topographic organization of respiratory responses to glutamate microstimulation of the parabrachial nucleus in the rat. J Neurosci 1994;14:6500-10.
92. Cohen MI. Switching of the respiratory phases and evoked phrenic responses produced by rostral pontine electrical stimulation. J Physiol 1971;217:133-58.
93. Lara JP, Parkes MJ, Silva-Carvhalo L, Izzo P, Dawid-Milner MS, Spyer KM. Cardiovascular and respiratory effects of stimulation of cell bodies of the parabrachial nuclei in the anaesthetized rat. J Physiol 1994;477 (Pt 2):321-9.
94. Song G, Poon CS. Lateral parabrachial nucleus mediates shortening of expiration during hypoxia. Respir Physiol Neurobiol 2009;165:1-8.

95. Christie MJ, North RA. Agonists at mu-opioid, M2-muscarinic and GABAB-receptors increase the same potassium conductance in rat lateral parabrachial neurones. Br J Pharmacol 1988;95:896-902.
96. Kabbaj M, Vachon P, Varin F. Impact of peripheral elimination on the concentration-effect relationship of remifentanil in anaesthetized dogs. Br J Anaesth 2005;94:357-65.
97. Poisnel G, Quentin T, Barre L, Coquerel A, Debruyne D. Competitive displacement binding assay on rat brain sections and using a beta-imager: application to mu-opioid ligands. J Neurosci Methods 2006;154:60-7.
98. Yassen A, Olofsen E, Dahan A, Danhof M. Pharmacokinetic-pharmacodynamic modeling of the antinociceptive effect of buprenorphine and fentanyl in rats: role of receptor equilibration kinetics. J Pharmacol Exp Ther 2005;313:1136-49.
99. Zadina JE, Hackler L, Ge LJ, Kastin AJ. A potent and selective endogenous agonist for the mu-opiate receptor. Nature 1997;386:499-502.
100. Krause KL, Neumueller SE, Marshall BD, et al. Micro-opioid receptor agonist injections into the presumed pre-Botzinger complex and the surrounding region of awake goats do not alter eupneic breathing. J Appl Physiol (1985) 2009;107:1591-9.
101. Pattinson KT, Governo RJ, MacIntosh BJ, et al. Opioids depress cortical centers responsible for the volitional control of respiration. J Neurosci 2009;29:8177-86.
102. Benarroch EE. Pain-autonomic interactions. Neurol Sci 2006;27 Suppl 2:S130-3.
103. Jiang M, Alheid GF, Calandriello T, McCrimmon DR. Parabrachial-lateral pontine neurons link nociception and breathing. Respir Physiol Neurobiol 2004;143:215-33.
104. Saper CB. The central autonomic nervous system: conscious visceral perception and autonomic pattern generation. Annu Rev Neurosci 2002;25:433-69.

9. CURRICULUM VITAE

Ivana Prkić, M.D.

Date and Place of Birth: November 14, 1985, Split, Croatia

Work Address:

Department of Anesthesiology, reanimatology and intensive care, University Hospital Split
Spinciceva 1
21000 Split, Croatia.

E-mail: ivana.prkich@gmail.com

Phone: +385 99 206 2020

EDUCATION:

2004-2010: University of Split, School of Medicine, Croatia
2010-2013: Postdoctoral Research Fellowship in Neurobiology and Neuropharmacology of Breathing, Medical College of Wisconsin, Milwaukee, WI, USA
May, 2014: Board exam, Split, Croatia
2014–present: Postgraduate school "Translational research in biomedicine (TRIBE)", University of Split, School of Medicine, Split, Croatia
November, 2014: Advanced Life Support course

WORK EXPERIENCE:

2010-2013: Postdoctoral research fellow, Medical College of Wisconsin, Milwaukee, WI, USA
2013-2014: Internship, Split, Croatia
8/2014: Family practice, Kastel Stari, Croatia
10/2014.-present: Resident at Department of anesthesiology, reanimatology and intensive care, University Hospital Split, Croatia

PUBLICATIONS:

1. **Prkic Ivana**, Mustapic Sanda, Radocaj Tomislav, Stucke Astrid G, Stuth Eckehard A.E, Hopp Francis A., Dean Caron, and Zuperku Edward J. Pontine μ-opioid receptors mediate the bradypnea caused by intravenous remifentanil infusions at clinically relevant concentrations in dogs. J Neurophysiol 2012; doi: 10.1152/jn.00185.2012.
2. Zuperku Edward J, **Prkic Ivana**, Stucke Astrid G, Miller Justin R, Hopp Francis A, Stuth Eckehard A.E. Automatic classification of canine PRG neuronal discharge patternsusing K-means clustering. Respir Physiol Neurobiol. 2015; doi: 10.1016/j.resp.2014.11.016
3. Stucke Astrid G, Miller J.R, **Prkic Ivana**, Zuperku Edward J, Hopp Francis A, Eckehard A.E. Opioid-induced Respiratory Depression Is Only Partially Mediated by the preBötzinger Complex in Young and Adult Rabbits In Vivo. Anesthesiology, March 2015;
4. Radocaj Tomislav, Mustapic Sanda, **Prkic Ivana**, Stucke Astrid G, Hopp Francis A., Stuth Eckehard A.E, and Zuperku Edward J. Activation of 5-HT1A receptors in the preBötzinger region has little impact on the respiratory pattern. Resp Physiol Neurobi, March 2015.

POSTERS AND PRESENTATIONS AT SCIENTIFIC MEETINGS:

1. Attended Experimental Biology 2011, Washington D.C., USA, April 2011.
2. **Ivana Prkic**, Sanda Mustapic, Tomislav Radocaj, Astrid G. Stucke, Eckehard A. E. Stuth, Francis A. Hopp, Caron Dean and Edward J. Zuperku. Pontine μ-opioid receptors mediate the bradypnea caused by clinically relevant rates of intravenous remifentanil in dogs. Experimental Biology 2012, San Diego, USA, April 2012.
3. Astrid G. Stucke, Edward J. Zuperku, Nicole M. Geissinger, Francis A. Hopp, **Ivana Prkic**, Eckehard A. E. Stuth. The effect of DAMGO on the preBötzinger Complex in young and adult rabbits. Experimental Biology 2012, San Diego, USA, April 2012.
4. **Ivana Prkic**, Sanda Mustapic, Tomislav Radocaj, Astrid G. Stucke, Eckehard A. E. Stuth, Francis A. Hopp, Caron Dean and Edward J. Zuperku. Pontine μ-opioid receptors mediate the bradypnea caused by clinically relevant rates of intravenous remifentanil in dogs. Research Day Abstract Poster Day 2012 MCW, Milwaukee, USA, September 2012.
5. Astrid G. Stucke, Edward J. Zuperku, **Ivana Prkic**, Nicole M. Geissinger, Eckehard A. E. Stuth. Intravenous Remifentanil Depresses Breathing *via* the preBötzinger Complex in Young but not in Adult Rabbits. American Society of Anesthesiologists 2012, Washington DC, October 2012.

6. **Ivana Prkic**, Sanda Mustapic, Tomislav Radocaj, Astrid G. Stucke, Eckehard A. E. Stuth, Francis A. Hopp, Caron Dean and Edward J. Zuperku. Pontine μ-opioid receptors mediate the bradypnea caused by clinically relevant rates of intravenous remifentanil in dogs. 22nd Annual Research Poster Session 2012, Milwaukee, USA, October 2012.
7. Astrid G. Stucke, Eckehard A.E. Stuth, **Ivana Prkic**, Caron Dean, Francis A. Hopp, Edward J. Zuperku. The Role of the preBötzinger Complex in Opioid-Induced Respiratory Depression is Age-Dependent**.** Association of University Anesthesiologists 60th Annual Meeting**,** Miami, USA, April 2013.
8. **Ivana Prkic**, Sanda Mustapic, Tomislav Radocaj, Astrid G. Stucke, Eckehard A. E. Stuth, Francis A. Hopp and Edward J. Zuperku. Effects of iv remifentanil on the discharge of canine pontine respiratory group (PRG) neurons in the parabrachial complex. Experimental Biology 2013, Boston, USA, April 2013.
9. Astrid G. Stucke, Edward J. Zuperku, Francis A. Hopp, **Ivana Prkic**, Eckehard A.E. Stuth. The PreBötzinger Complex Partially Mediates Opioid-Induced Respiratory Depression in Young but not in Adult Rabbits. Experimental Biology 2013, Boston, USA, April 2013.
10. Edward J. Zuperku, **Ivana Prkic**, Francis A. Hopp, Justin R. Miller, Astrid G. Stucke, Eckehard A. Stuth. A subregion within the pontine parabrachial complex plays a key role in the control of breathing frequency. Presentation Experimental Biology 2014, San Diego, USA, April 2014.
11. Edward J. Zuperku, **Ivana Prkic**, Francis A. Hopp, Justin R. Miller, Astrid G. Stucke, Eckehard A. Stuth. Pontine respiratory group (PRG) neuronal discharge is modulated by powerful GABAergic tonic inhibition. Experimental Biology 2014, San Diego, USA, April 2014.
12. Edward J. Zuperku, **Ivana Prkic**, Francis A. Hopp, Justin R. Miller, Astrid G. Stucke, Eckehard A. Stuth. Relative contributions of NMDA and AMPA receptor-mediated excitation to the spontaneous discharge of canine pontine respiratory group (PRG) neurons. Experimental Biology 2014, San Diego, USA, April 2014.

ORAL PRESENTATIONS:

1. **Ivana Prkić**, Brainstem location of μ-opioid receptors underlying respiratory depression, Anesthesiology Department seminar, Medical College of Wisconsin, Milwaukee, WI, USA, June 2012.
2. **Ivana Prkić,** Opioids and control of breathing, University of Split, School of Medicine, Split, Croatia, September 2013.

MEMBERSHIP:

Member of the Croatian Medical Association.